Comput. Methods Appl. Mech. Engrg. 200 (2011) 2094–2116

Contents lists available at ScienceDirect

Comput. Methods Appl. Mech. Engrg.

journal homepage: www.elsevier.com/locate/cma

Stability and convergence of sequential methods for coupled flow and geomechanics: Drained and undrained splits

J. Kim [a,b], H.A. Tchelepi [a], R. Juanes [c,*]

[a] Department of Energy Resources Engineering, Stanford University, Green Earth Sciences Building, 367 Panama Street, Stanford, CA 94305, USA
[b] Earth Sciences Division, Lawrence Berkeley National Laboratory, 1 Cyclotron Road 90R1116, Berkeley, CA 94720, USA
[c] Department of Civil and Environmental Engineering, Massachusetts Institute of Technology, 77 Massachusetts Avenue, Building 48-319, Cambridge, MA 02139, USA

ARTICLE INFO

Article history:
Received 6 November 2009
Received in revised form 21 October 2010
Accepted 9 February 2011
Available online 2 March 2011

Keywords:
Geomechanics
Poromechanics
Stability analysis
Convergence analysis
Drained split
Undrained split

ABSTRACT

We perform a stability and convergence analysis of sequential methods for coupled flow and geomechanics, in which the mechanics sub-problem is solved first. We consider slow deformations, so that inertia is negligible and the mechanical problem is governed by an elliptic equation. We use Biot's self-consistent theory to obtain the classical parabolic-type flow problem. We use a generalized midpoint rule (parameter α between 0 and 1) time discretization, and consider two classical sequential methods: the drained and undrained splits.

The von Neumann method provides sharp stability estimates for the linear poroelasticity problem. The drained split with backward Euler time discretization ($\alpha = 1$) is conditionally stable, and its stability depends only on the coupling strength, and it is independent of time step size. The drained split with the midpoint rule ($\alpha = 0.5$) is unconditionally unstable. The mixed time discretization, with $\alpha = 1.0$ for mechanics and $\alpha = 0.5$ for flow, has the same stability properties as the backward Euler scheme. The von Neumann method indicates that the undrained split is unconditionally stable when $\alpha \geqslant 0.5$.

We extend the stability analysis to the nonlinear regime (poro-elastoplasticity) via the energy method. It is well known that the drained split does not inherit the contractivity property of the continuum problem, thereby precluding unconditional stability. For the undrained split we show that it is B-stable (therefore unconditionally stable at the algorithmic level) when $\alpha \geqslant 0.5$.

We also analyze convergence of the drained and undrained splits, and derive the *a priori* error estimates from matrix algebra and spectral analysis. We show that the drained split with a fixed number of iterations is not convergent even when it is stable. The undrained split with a fixed number of iterations is convergent for a compressible system (i.e., finite Biot modulus). For a nearly-incompressible system (i.e., very large Biot modulus), the undrained split loses first-order accuracy, and becomes non-convergent in time.

We also study the rate of convergence of both splits when they are used in a fully-iterated sequential scheme. When the medium permeability is high or the time step size is large, which corresponds to a high diffusion of pressure, the error amplification of the drained split is lower and therefore converges faster than the undrained split. The situation is reversed in the case of low permeability and small time step size.

We provide numerical experiments supporting all the stability and convergence estimates of the drained and undrained splits, in the linear and nonlinear regimes. We also show that our spatial discretization (finite volumes for flow and finite elements for mechanics)removes the well-documented spurious instability in consolidation problems at early times..

1. Introduction

The study of coupled fluid or heat flow and mechanics is important in many fields of science and engineering. Heat can extend or shrink bodies, and the thermal stress by heating can affect, in turn, body deformation [1]. Coupling of flow and mechanics has far-reaching consequences for soft tissues such as blood cells [2] and the brain, whose mechanical response depends critically on hydration [3]. In geotechnical and geological settings, an increase in pore pressure leads to a reduction of effective stress [4–6], which may affect the stability of fractures and faults [7–11]. In petroleum engineering, reservoir geomechanics plays a crucial role in production

* Corresponding author. Tel.: +1 617 253 7191.
E-mail addresses: JihoonKim@lbl.gov (J. Kim), tchelepi@stanford.edu (H.A. Tchelepi), juanes@mit.edu (R. Juanes).

0045-7825/$ - see front matter © 2011 Elsevier B.V. All rights reserved.
doi:10.1016/j.cma.2011.02.011

by compaction drive [12], surface subsidence [13], caprock integrity, and well failure [14,15].

Two basic strategies exist to solve the coupled flow and geomechanics problem: a fully coupled approach, and a sequential solution approach [16–23]. In the fully coupled method, the governing equations of flow and geomechanics are solved simultaneously at every time step. A converged solution is obtained through iteration, typically using the Newton–Raphson method [9,23–26]. This approach is unconditionally stable, but requires the development of a unified flow–geomechanics simulator and can be computationally expensive.

In the sequential approach, either the flow or mechanical problem is solved first, then the other problem is solved using the intermediate solution information [16–18,20,21,23,27]. One may iterate this sequential procedure at each time step until convergence – the solution is then identical to that obtained using the fully coupled approach – or perform a fixed number of iterations per time step – it is common to employ a staggered solution strategy with only one iteration per time step [26,28–33].

This partitioned approach offers several advantages. The most important advantage is that a sequential approach makes use of existing simulation codes for flow and mechanics, and only the interface between those codes needs to be implemented [34,16]. One can then enjoy the efficiency and wide flexibility in terms of software engineering. Despite these desirable features, the use of sequential schemes may be limited by the lack of stability and convergence of the overall operator split.

1.1. Previous work

Stability. Significant efforts to find stable and efficient sequential methods for coupled poromechanics (or the analogous thermomechanics problem) have been pursued in the geotechnical and computational mechanics communities [26,28–30,33,35,36]. Most of these methods assume that the mechanical subproblem is solved first. Two sequential schemes are relevant here. One is the drained split method (the isothermal split in the thermomechanical problem [30]), and the other one is the undrained split method [23,26,29] (the adiabatic split in the thermomechanical problem [30]). The drained method freezes the pressure during the mechanical step. It is well-known that, despite its simplicity, this scheme is only conditionally stable [28–30]. The undrained method, on the other hand, freezes the fluid mass content when solving the mechanics problem. It has been shown that this split respects the dissipative structure of the continuum problem [30]. The undrained method can be applied to linear coupled problems [23,29,33,35] as well as nonlinear problems [26].

To show unconditional stability of a sequential method via the energy method, the following three steps must be taken [30,37–40]:

1. Determine whether the continuum problem is contractive. The appropriate norm to show contractivity (non-negative energy dissipation) is defined at this step.
2. Show that the operator split corresponding to the sequential method honors, at the continuum level, the contractivity property relative to the norm defined in the previous step. If the operator split is not contractive, it is not possible to obtain an unconditionally stable method [41].
3. When the operator split is contractive at the continuum level, one must then show contractivity at the discrete time level (B-stability) for the individual subproblems with a specific time discretization (e.g., backward Euler or midpoint rule). The algorithmic stability of the subproblems for an uncoupled problem is not applicable to the study of the stability of the coupled problem because the natural norms of the subproblems are different from that of the coupled problem.

Contractivity of the problem (Step 1) and the undrained-split operator (Step 2) has been rigorously shown for the thermomechanics problem by Armero and Simo [30]. Following this work, Romero [40] introduced the midpoint rule as an unconditionally stable time-stepping algorithm for thermoelasticity (Step 3). The focus of these works is on thermomechanical problems with fully-dynamic (inertial) mechanics, and leave open several important questions regarding the stability and convergence of sequential schemes for coupled flow and *quasi-static* mechanics. Quasi-static mechanics produces differential algebraic equations (DAEs) as a semi-discrete version of the partial differential equation (PDE), whereas fully-dynamic mechanics produces ordinary differential equations (ODEs). Indeed, ODEs and DAEs generally exhibit different numerical convergence behavior [42].

Armero and Simo [30] do separately investigate the stability of the drained and undrained splits for quasi-static mechanics, but only as an illustrative calculation based on two degrees of freedom (one wave number), and later Armero [26] proves that the undrained split is thermodynamically consistent. However, a complete analysis leading to sharp stability criteria and B-stability for coupled flow and quasi-static mechanics is still missing.

Convergence. Stability, in general, does not guarantee convergence. While the fully coupled method with a backward Euler time stepping is typically first-order convergent with respect to time, the convergence properties of sequential schemes depend strongly on the details of the splitting strategy, the specific form and discretization schemes used for the various subproblems, and how the subproblems communicate during a time step.

Consider a continuum operator $\mathcal{A}$ that can be additively split as:

$$\dot{\mathbf{y}}(t) = \mathcal{A}\mathbf{y}(t) = (\mathcal{A}_1 + \mathcal{A}_2)\mathbf{y}(t), \tag{1}$$

where $\mathcal{A}$ can be linear, or nonlinear, $\mathbf{y}$ is a solution vector, and $\dot{(\,)}$ is the time derivative. We solve two subproblems in sequence as follows:

$$\underbrace{\dot{\mathbf{y}}(t) = \mathcal{A}_1\mathbf{y}(t)}_{\text{problem 1}} \quad \text{and} \quad \underbrace{\dot{\mathbf{y}}(t) = \mathcal{A}_2\mathbf{y}(t)}_{\text{problem 2}}. \tag{2}$$

In this case, even when one iteration is performed (i.e., a staggered method), the sequential method from Eq. (2) is convergent by Lie's formula [43,44]. When the operator splitting of Eq. (2) is applied to the coupled heat flow and mechanical-dynamics, convergence with first-order accuracy in time is obtained, as long as the discrete algorithm is stable [30].

In general, however, sequential methods with a fixed number of iterations do not guarantee convergence, even when they are numerically stable [45]. Operator splitting of coupled flow and geomechanics, where the mechanical problem is quasi-static, can be written as:

$$\underbrace{0 = \mathcal{A}_1\mathbf{y}(t)}_{\text{mechanics}} \quad \text{and} \quad \underbrace{0 = \mathcal{A}_2(\mathbf{y}(t), \dot{\mathbf{y}}(t))}_{\text{flow}}. \tag{3}$$

Lie's formula cannot be applied to Eq. (3), and it is unclear whether sequential methods are convergent for a fixed iteration number, even when they are stable. It was mentioned by Armero [26] that the undrained split may suffer from loss of accuracy for strongly coupled problems, but a comprehensive analysis is missing. The convergence of sequential methods with a fixed iteration number is important, since a fixed iteration number is typically required in order to save computational resources.

Vijalapura and Govindjee [46] propose a hybrid scheme of staggered and fully coupled methods, in which the time step size is controlled for accuracy based on the assumption that refining the time step size improves the accuracy of the staggered method. Vijalapura et al. [47] investigate the order of accuracy of index-1 differential algebraic equations of the type given in Eq. (3) where

the mechanical problem can be viewed as an algebraic constraint [42]. They find that sequential methods of the differential algebraic equations have first-order accuracy when the first step in the algebraic equation is redundant. However, this is not applicable to the coupled flow and quasi-static mechanics because the mechanical problem is not redundant for the first time step: consolidation problems are often driven by instant loading in the mechanical problem during the first time step. In fact, the work of Vijalapura et al. [47] supports the fact that typical sequential methods are non-convergent in time when the first step in the algebraic equation is not redundant.

1.2. Summary of results

With the above issues in mind, in this paper we focus on the stability and convergence analysis for the drained and undrained splits. First, we perform a comprehensive stability analysis of the drained and undrained splits for coupled flow and *quasi-static* geomechanics with a generalized midpoint rule time discretization (evaluation at time $t_{n+\alpha}$, with $\alpha \in [0,1]$). Following Armero and Simo [30], we use the von Neumann method to analyze the linear problem, and the energy method for the nonlinear problem.

Our von Neumann analysis leads to sharper stability estimates than previously found [30] (the focus of [30] was on the fully-dynamic case, and the stability estimate for the quasi-static case was just a side calculation using two degrees of freedom). We determine stringent bounds for stability of the drained split. For instance, we find it is unconditionally unstable when the midpoint rule is used ($\alpha = 0.5$). Even when the backward Euler time-stepping is used ($\alpha = 1$), the stability of the drained split is delicate: it depends only on the coupling strength between flow and mechanics, and (rather surprisingly) it is independent of time step size. Moreover, when it is stable, it yields an oscillatory solution. In contrast, the von Neumann analysis shows that the undrained split is unconditionally stable for $\alpha \geqslant 0.5$.

We provide a complete stability analysis of the undrained split for the nonlinear problem, following the analysis of Armero and Simo [30] and Armero [26] and extending it to the fully algorithmic (time-discrete) problem. We show, following the analysis of Simo [37] and Simo and Govindjee [48] for the uncoupled problem, that the undrained split is unconditionally stable if $\alpha \geqslant 0.5$.

We then investigate the convergence of the drained and undrained splits under the backward Euler time-stepping method. We obtain *a priori* error estimates for the two sequential methods using matrix algebra, which is similar to the method by Turska et al. [45], and spectral analysis. We show that the drained split with a fixed number of iterations is not convergent, and that the undrained split with a fixed iteration number is convergent for a compressible system and non-convergent for an incompressible system.

From a spectral analysis, the error amplification factors between two sequential schemes and the fully coupled method allow us to estimate the rate of convergence when the sequential schemes are fully-iterated at each time step. Schrefler et al. [49] use the spectral radii of error amplification matrix to investigate the rate of convergence for the staggered Newton schemes based on the drained split. They show in the numerical study of a 1-D model with two degrees of freedom that the spectral radii of the error amplification matrix decrease as the time step size increases, which explains the fast convergence rate.

Here, we obtain analytical estimates for the error amplification factors, which provide similar information to the spectral radii of error amplification matrix: smaller values indicate faster rate of convergence [49]. Thus, the analytic derivation of the error amplification factors provides *a priori* estimates of the rate of convergence for the drained and undrained splits. In this paper we show that the error amplification factor of the drained split decreases when permeability is high and time step size is large (i.e. high diffusivity of pressure). In contrast, convergence of the undrained split is fast in the case of low permeability and small time step size (i.e. low diffusivity of pressure).

We perform numerical simulations that support the results from the stability and convergence analysis. We use a finite volume method for the flow equation and a finite element method for the mechanics. This mixed space discretization method is locally mass conservative (see also [23]), and is effective at eliminating the instability at early time for consolidation problems with compressible fluids [50–54].

2. Mathematical model

We adopt a classical continuum representation, where fluid and solid are viewed as overlapping continua. The physical model is based on the poroelasticity and poroelastoplasticity theories (see, e.g., [5]). In this paper, we assume isothermal single-phase flow of a slightly compressible fluid, small deformation (i.e., infinitesimal transformations), isotropic material, and no stress-dependence of flow properties like porosity or permeability. The governing equations for coupled flow and reservoir geomechanics come from the mass balance and linear momentum balance. Under the quasi-static assumption for solid displacements, the governing equation for mechanical deformation of the solid–fluid system can be expressed as:

$$\mathrm{Div}\,\boldsymbol{\sigma} + \rho_b \boldsymbol{g} = \mathbf{0}, \tag{4}$$

where Div $(\cdot)$ is the divergence operator, $\boldsymbol{\sigma}$ is the Cauchy total stress tensor, $\boldsymbol{g}$ is the gravity vector, $\rho_b = \phi\rho_f + (1-\phi)\rho_s$ is the bulk density, ρ_f is fluid density, ρ_s is the density of the solid phase, and ϕ is the true porosity. The true porosity is defined as the ratio of the pore volume and the bulk volume in the deformed configuration. A stress–strain relation must be specified for the mechanical behavior of the porous medium. Changes in total stress and fluid pressure are related to changes in strain and fluid content by Biot's theory [4,5,25,55,56]. In the form of Biot's theory [5], the poroelasticity equations take the following form:

$$\boldsymbol{\sigma} - \boldsymbol{\sigma}_0 = \mathbf{C}_{dr} : \boldsymbol{\varepsilon} - b(p - p_0)\mathbf{1}, \tag{5}$$

$$\frac{1}{\rho_{f,0}}(m - m_0) = b\varepsilon_v + \frac{1}{M}(p - p_0), \tag{6}$$

where the subscript 0 means reference state, $\mathbf{C}_{dr}$ is the rank-4 drained elasticity tensor, $\mathbf{1}$ is the rank-2 identity tensor, p is fluid pressure, m is fluid mass per unit bulk volume, M is the Biot modulus, and b is the Biot coefficient. Note that we use the convention that tensile stress is positive. Here, $\boldsymbol{\varepsilon}$ is the linearized strain tensor under the assumption of infinitesimal transformation:

$$\boldsymbol{\varepsilon} = \mathbf{Grad}^s \boldsymbol{u} = \frac{1}{2}\left(\mathbf{Grad}\ \boldsymbol{u} + \mathbf{Grad}^t\ \boldsymbol{u}\right). \tag{7}$$

Note that we also have [5]:

$$\frac{1}{M} = \phi_0 c_f + \frac{b - \phi_0}{K_s}, \tag{8}$$

$$b = 1 - \frac{K_{dr}}{K_s}, \tag{9}$$

where c_f is the fluid compressibility $(1/K_f)$, K_f is the bulk modulus of the fluid, K_s is the bulk modulus of the solid grain, and K_{dr} is the drained bulk modulus. It is convenient to express the strain and stress tensors in terms of their volumetric and deviatoric parts:

$$\boldsymbol{\varepsilon} = \frac{1}{3}\varepsilon_v \mathbf{1} + \boldsymbol{e}, \tag{10}$$

$$\boldsymbol{\sigma} = \sigma_v \mathbf{1} + \boldsymbol{s}, \tag{11}$$

where $\varepsilon_v = \mathrm{tr}\,\boldsymbol{\varepsilon}$ is the volumetric strain (the trace of the strain tensor), $\boldsymbol{e}$ is the deviatoric part of the strain tensor, $\sigma_v = \frac{1}{3}\mathrm{tr}\,\boldsymbol{\sigma}$ is the volumetric (mean) total stress, and $\boldsymbol{s}$ is the deviatoric total stress tensor.

Under the assumption of small deformations, the fluid mass conservation equation is

$$\frac{\partial m}{\partial t} + \mathrm{Div}\,\boldsymbol{w} = \rho_{f,0} f, \tag{12}$$

where $\boldsymbol{w}$ is the fluid mass flux (fluid mass flow rate per unit area and time), and f is a volumetric source term. Using Eq. (6), we write Eq. (12) in terms of pressure and volumetric strain:

$$\frac{1}{M}\frac{\partial p}{\partial t} + b\frac{\partial \varepsilon_v}{\partial t} + \mathrm{Div}\,\frac{\boldsymbol{w}}{\rho_{f,0}} = f. \tag{13}$$

The relation between volumetric stress and strain reads:

$$(\sigma_v - \sigma_{v,0}) + b(p - p_0) = K_{dr}\varepsilon_v. \tag{14}$$

The fluid velocity $\boldsymbol{v} = \boldsymbol{w}/\rho_{f,0}$ is given by Darcy's law:

$$\boldsymbol{v} = -\frac{\boldsymbol{k}}{\mu}\left(\mathbf{Grad}\; p - \rho_f \boldsymbol{g}\right), \tag{15}$$

where $\boldsymbol{k}$ is the positive-definite absolute permeability tensor, and μ is the fluid viscosity.

To complete the description of the coupled flow and geomechanics mathematical problem, we need to specify initial and boundary conditions. For the flow problem we consider the boundary conditions $p = \bar{p}$ (prescribed pressure) on Γ_p, and $\boldsymbol{v}\cdot\boldsymbol{n} = \bar{v}$ (prescribed volumetric flux) on Γ_v, where $\boldsymbol{n}$ is the outward unit normal to the boundary, $\partial\Omega$. For well-posedness of the problem, we assume that $\Gamma_p \cap \Gamma_v = \emptyset$, and $\Gamma_p \cup \Gamma_v = \partial\Omega$.

The boundary conditions for the mechanical problem are $\boldsymbol{u} = \bar{\boldsymbol{u}}$ (prescribed displacement) on Γ_u and $\boldsymbol{\sigma}\cdot\boldsymbol{n} = \bar{\boldsymbol{t}}$ (prescribed traction) on Γ_σ. Again, we assume $\Gamma_u \cap \Gamma_\sigma = \emptyset$, and $\Gamma_u \cup \Gamma_\sigma = \partial\Omega$.

The initial displacements and strains are, by definition, equal to zero. The initial condition of the coupled problem is $p|_{t=0} = p_0$ and $\boldsymbol{\sigma}|_{t=0} = \boldsymbol{\sigma}_0$. The initial stress field should satisfy mechanical equilibrium, and reflect the history of stress paths in the formation of the reservoir. Initialization of the geomechanical model is a difficult task in itself [15].

3. Discretization

Traditional reservoir simulation is based on the finite volume method [57], whereas the computational mechanics community has favored the use of finite element discretizations [9,24–26,29,30,52]. Here, we use a mixed discretization that employs a finite volume method for the flow problem and a nodal-based finite element method for the mechanical problem. The pressure unknown is located at the element center, and the displacement vector is located at element vertices [58]. This space discretization is locally mass conservative at the element level, yields a continuous displacement field and enjoys excellent stability properties [23,59].

Let the domain be partitioned into nonoverlapping elements, $\Omega = \cup_{j=1}^{n_{\mathrm{elem}}}\Omega_j$, where n_{elem} is the number of elements. Let $\mathcal{Q} \subset L^2(\Omega)$ and $\mathcal{U} \subset (H^1(\Omega))^d$ (where $d = 2, 3$ is the number of space dimensions), be the functional spaces of the solution for pressure, p, and displacements, $\boldsymbol{u}$. Let $\mathcal{Q}_0$ and $\mathcal{U}_0$ be the corresponding function spaces for the test functions φ and $\boldsymbol{\eta}$, for flow and mechanics, respectively. Let $\mathcal{Q}_h$, $\mathcal{Q}_{h,0}$, $\mathcal{U}_h$ and $\mathcal{U}_{h,0}$ be the corresponding finite-dimensional subspaces. Then, the discrete approximation of the weak form of the governing Eqs. (4) and (12) becomes: find $(\boldsymbol{u}_h, p_h) \in \mathcal{U}_h \times \mathcal{Q}_h$ such that:

$$\int_\Omega \mathbf{Grad}^{\mathrm{s}}\boldsymbol{\eta}_h : \boldsymbol{\sigma}_h\, d\Omega = \int_\Omega \boldsymbol{\eta}_h\cdot\rho_b\boldsymbol{g}\, d\Omega + \int_{\Gamma_\sigma}\boldsymbol{\eta}_h\cdot\bar{\boldsymbol{t}}\, d\Gamma \quad \forall\boldsymbol{\eta}_h \in \mathcal{U}_{h,0}, \tag{16}$$

$$\frac{1}{\rho_{f,0}}\int_\Omega \varphi_h\frac{\partial m_h}{\partial t}\, d\Omega + \int_\Omega \varphi_h \mathrm{Div}\,\boldsymbol{v}_h\, d\Omega = \int_\Omega \varphi_h f\, d\Omega, \quad \forall\varphi_h \in \mathcal{Q}_{h,0}. \tag{17}$$

The pressure and displacement fields are approximated as follows:

$$p_h = \sum_{j=1}^{n_{\mathrm{elem}}}\varphi_j P_j, \tag{18}$$

$$\boldsymbol{u}_h = \sum_{b=1}^{n_{\mathrm{node}}}\eta_b \boldsymbol{U}_b, \tag{19}$$

where n_{node} is the number of nodes, P_j are the element pressures, and $\boldsymbol{U}_b$ are the displacement vectors at the element nodes (vertices). We restrict our analysis to pressure shape functions that are piecewise constant functions, so that φ_j takes a constant value of 1 over element j and 0 at all other elements. Therefore, Eq. (17) can be interpreted as a mass conservation statement element-by-element. The second term can be integrated by parts to arrive at the sum of integral fluxes, $V_{h,ij}$, between element i and its adjacent elements j:

$$\int_\Omega \varphi_i \mathrm{Div}\,\boldsymbol{v}_h\, d\Omega = -\int_{\partial\Omega_i}\boldsymbol{v}_h\cdot\boldsymbol{n}_i\, d\Gamma = -\sum_{j=1}^{n_{\mathrm{face}}}\int_{\Gamma_{ij}}\boldsymbol{v}_h\cdot\boldsymbol{n}_i\, d\Gamma = -\sum_{j=1}^{n_{\mathrm{face}}}V_{h,ij}. \tag{20}$$

The inter-element flux can be evaluated using a two-point or a multipoint flux approximation [60].

The displacement interpolation functions are the usual C^0–continuous isoparametric functions, such that η_b takes a value of 1 at node b, and 0 at all other nodes [58]. Inserting the interpolation from Eqs. (18), (19), and testing Eqs. (16), (17) against each individual shape function, the semi-discrete finite-element/finite-volume equations read:

$$\int_\Omega \boldsymbol{B}_a^T\boldsymbol{\sigma}_h\, d\Omega = \int_\Omega \eta_a\rho_b\boldsymbol{g}\, d\Omega + \int_{\Gamma_\sigma}\eta_a\bar{\boldsymbol{t}}\, d\Gamma \quad \forall a = 1,\ldots,n_{\mathrm{node}}, \tag{21}$$

$$\int_{\Omega_i}\frac{1}{M}\frac{\partial P_i}{\partial t}\, d\Omega + \int_{\Omega_i} b\frac{\partial\varepsilon_v}{\partial t}\, d\Omega - \sum_{j=1}^{n_{\mathrm{face}}}V_{h,ij} = \int_{\Omega_i} f\, d\Omega, \quad \forall i = 1,\ldots,n_{\mathrm{elem}}. \tag{22}$$

The matrix $\boldsymbol{B}_a$ is the linearized strain operator, which in 2D takes the form:

$$\boldsymbol{B}_a = \begin{bmatrix} \partial_x\eta_a & 0 \\ 0 & \partial_y\eta_a \\ \partial_y\eta_a & \partial_x\eta_a \end{bmatrix}. \tag{23}$$

The stress and strain tensors are expressed in compact engineering notation [58]. For example, in 2D:

$$\boldsymbol{\sigma}_h = \begin{bmatrix}\sigma_{h,xx}\\ \sigma_{h,yy}\\ \sigma_{h,xy}\end{bmatrix}, \quad \boldsymbol{\varepsilon}_h = \begin{bmatrix}\varepsilon_{h,xx}\\ \varepsilon_{h,yy}\\ 2\varepsilon_{h,xy}\end{bmatrix}. \tag{24}$$

The stress–strain relation for linear poroelasticity takes the form:

$$\boldsymbol{\sigma}_h = \boldsymbol{\sigma}'_h - bp_h\mathbf{1}, \quad \delta\boldsymbol{\sigma}'_h = \boldsymbol{D}\delta\boldsymbol{\varepsilon}_h, \tag{25}$$

where $\boldsymbol{\sigma}'$ is the effective stress tensor, and $\boldsymbol{D}$ is the elasticity matrix which, for 2D plane strain conditions, reads [58]:

$$\boldsymbol{D} = \frac{E(1-\nu)}{(1+\nu)(1-2\nu)}\begin{bmatrix} 1 & \frac{\nu}{1-\nu} & \frac{\nu}{1-\nu} \\ \frac{\nu}{1-\nu} & 1 & \frac{\nu}{1-\nu} \\ \frac{\nu}{1-\nu} & \frac{\nu}{1-\nu} & 1 \end{bmatrix}, \tag{26}$$

where E is Young's modulus, and ν is the drained Poisson ratio.

The coupled equations of quasi-static poromechanics form an elliptic–parabolic system of equations. A fully discrete system of equations can be obtained by further discretizing in time the mass

accumulation term in Eqs. (21) and (22). In this paper, we use the generalized midpoint rule (with $\alpha \in [0,1]$).

4. Operator splitting

The fully coupled method solves the equations of flow and mechanics simultaneously, and obtains a converged solution through iteration, typically using the Newton–Raphson method [24,25]. Let us denote by $\mathcal{A}$ the operator of the original problem (Eqs. (4) and (12)). The discrete approximation of this operator corresponding to the fully coupled method can be represented as [59]:

$$\begin{bmatrix} \boldsymbol{u}^n \\ \boldsymbol{p}^n \end{bmatrix} \overset{\mathcal{A}_{fc}}{\rightarrow} \begin{bmatrix} \boldsymbol{u}^{n+1} \\ \boldsymbol{p}^{n+1} \end{bmatrix}, \quad \text{where } \mathcal{A}_{fc} : \begin{cases} \operatorname{Div}\boldsymbol{\sigma} + \rho_b \boldsymbol{g} = \boldsymbol{0}, \\ \dot{m} + \operatorname{Div}\boldsymbol{w} - \rho_{f,0} f = 0, \end{cases} \tag{27}$$

where $\dot{(\,)}$ denotes time derivative and the superscript n denotes time level t_n.

4.1. Drained split

In this scheme, the solution is obtained sequentially by first solving the mechanics problem, and then the flow problem. The pressure field is frozen when the mechanical problem is solved. The drained-split approximation of the operator $\mathcal{A}$ can be written as:

$$\begin{bmatrix} \boldsymbol{u}^n \\ \boldsymbol{p}^n \end{bmatrix} \overset{\mathcal{A}^u_{dr}}{\rightarrow} \begin{bmatrix} \boldsymbol{u}^{n+1} \\ \boldsymbol{p}^n \end{bmatrix} \overset{\mathcal{A}^p_{dr}}{\rightarrow} \begin{bmatrix} \boldsymbol{u}^{n+1} \\ \boldsymbol{p}^{n+1} \end{bmatrix},$$
$$\text{where } \begin{cases} \mathcal{A}^u_{dr} : \operatorname{Div}\boldsymbol{\sigma} + \rho_b \boldsymbol{g} = \boldsymbol{0}, \quad \delta p = 0, \\ \mathcal{A}^p_{dr} : \dot{m} + \operatorname{Div}\boldsymbol{w} - \rho_{f,0} f = 0, \quad \delta\boldsymbol{\varepsilon} = \boldsymbol{0}. \end{cases} \tag{28}$$

One solves the mechanical problem with no pressure change, then the fluid flow problem is solved with a frozen displacement field. In this scheme, the fluid is allowed to flow when the mechanical problem is solved [26].

4.2. Undrained split

The undrained split uses a different pressure predictor for the mechanical problem, which is computed by imposing that the fluid mass in each grid block remain constant during the mechanical step ($\delta m = 0$). The original operator $\mathcal{A}$ is split as follows:

$$\begin{bmatrix} \boldsymbol{u}^n \\ \boldsymbol{p}^n \end{bmatrix} \overset{\mathcal{A}^u_{ud}}{\rightarrow} \begin{bmatrix} \boldsymbol{u}^{n+1} \\ \boldsymbol{p}^* \end{bmatrix} \overset{\mathcal{A}^p_{ud}}{\rightarrow} \begin{bmatrix} \boldsymbol{u}^{n+1} \\ \boldsymbol{p}^{n+1} \end{bmatrix},$$
$$\text{where } \begin{cases} \mathcal{A}^u_{ud} : \operatorname{Div}\boldsymbol{\sigma} + \rho_b \boldsymbol{g} = \boldsymbol{0}, \ \delta m = 0, \\ \mathcal{A}^p_{ud} : \dot{m} + \operatorname{Div}\boldsymbol{w} - \rho_{f,0} f = 0, \ \delta\boldsymbol{\varepsilon} = \boldsymbol{0}. \end{cases} \tag{29}$$

The undrained split allows the pressure to change locally when the mechanical problem is solved. From Eq. (6), the undrained condition ($\delta m = 0$) yields:

$$0 = b\delta\varepsilon_v + \frac{1}{M}\delta p, \tag{30}$$

and the pressure is updated locally in each element using:

$$p^* = p^n - bM\left(\varepsilon_v^{n+1} - \varepsilon_v^n\right). \tag{31}$$

For the mechanical problem, Eq. (5) with the generalized midpoint rule at $t_{n+\alpha}$ is discretized as follows:

$$\boldsymbol{\sigma}^{n+\alpha} - \boldsymbol{\sigma}_0 = \mathbf{C}_{dr} : \boldsymbol{\varepsilon}^{n+\alpha} - b(p^{n+\alpha} - p_0)\mathbf{1}, \quad p^{n+\alpha} = \alpha p^* + (1-\alpha)p^n, \tag{32}$$

where $\alpha \in [0,1]$. After substituting Eq. (31) in Eq. (32), the mechanical problem can be expressed in terms of displacements using the undrained bulk modulus [26], $\mathbf{C}_{ud} = \mathbf{C}_{dr} + b^2 M \mathbf{1} \otimes \mathbf{1}$. The additional computational cost is negligible because the calculation of $\boldsymbol{p}^*$ is explicit.

5. Stability analysis for linear poroelasticity

We adopt the von Neumann method to analyze the stability of the different sequential schemes. This is a standard technique [61,62], which consists in examining the unbounded growth or decay of the Fourier representation of the numerical error.

We discretize the governing equations in one dimension and without source terms for space using second-order finite volume method for flow, and C^0 linear finite elements for mechanics. Despite the one dimensional analysis, the error estimation can be extended to multiple dimensions because the coupling between flow and mechanics is based on the volumetric response, which is a scalar quantity. We label the elements with index j. The nodes bounding element j are labeled with a half-index: $j-\frac{1}{2}$ and $j+\frac{1}{2}$. We denote the pressure unknown at element j by P_j^n and the displacement unknown at node $j+\frac{1}{2}$ by $U^n_{j+\frac{1}{2}}$, where n is the time level. We use a generalized midpoint rule, so the unknowns are evaluated at time $t_{n+\alpha}$ as $P^{n+\alpha} = \alpha P^{n+1} + (1-\alpha)P^n$ and $U^{n+\alpha} = \alpha U^{n+1} + (1-\alpha)U^n$. Let h be the element size, and Δt the time step size, both assumed constant. The fully discrete equations in 1D are:

$$\frac{K_{dr}}{h}\left(U^{n+\alpha}_{j-\frac{3}{2}} - 2U^{n+\alpha}_{j-\frac{1}{2}} + U^{n+\alpha}_{j+\frac{1}{2}}\right) + b\left(P^{n+\alpha}_{j-1} - P^{n+\alpha}_j\right) = 0, \tag{33}$$

$$\frac{h}{M}\frac{P_j^{n+1} - P_j^n}{\Delta t} + \frac{bh}{\Delta t}\left(-\frac{U^{n+1}_{j-\frac{1}{2}} - U^{n+1}_{j+\frac{1}{2}}}{h} + \frac{U^n_{j-\frac{1}{2}} - U^n_{j+\frac{1}{2}}}{h}\right) - \frac{k_p}{\mu h}\left(P^{n+\alpha}_{j-1} - 2P^{n+\alpha}_j + P^{n+\alpha}_{j+1}\right) = 0, \tag{34}$$

where k_p is the medium permeability.

It is known that the fully coupled method is unconditionally stable for $\alpha \geqslant 0.5$ [59,63]. In this section, we perform a von Neumann stability analysis for the drained and undrained sequential schemes.

5.1. Drained split

The drained split freezes the variation of the pressure during the mechanical step. Therefore, $P^{n+\alpha}$ is replaced by P^n in Eq. (33). We now introduce solutions of the form:

$$U^n_a = \gamma^n \exp(ia\theta)\widehat{U}, \tag{35}$$

$$P^n_j = \gamma^n \exp(ij\theta)\widehat{P}, \tag{36}$$

where γ is the amplification factor (γ^n means γ "to the power n"), i is the imaginary unit, and $\theta \in [-\pi, \pi]$. Since a is the node index, it takes values $j \mp \frac{1}{2}$, $j \mp \frac{3}{2}$, etc.

Substituting Eqs. (35), (36) into the discretized equations of the drained split, we obtain:

$$\underbrace{\begin{bmatrix} \frac{K_{dr}}{h}((1-\alpha)+\alpha\gamma)2(1-\cos\theta) & b2i\sin\frac{\theta}{2} \\ b(\gamma-1)2i\sin\frac{\theta}{2} & \frac{h}{M}(\gamma-1) + \frac{k_p\Delta t}{\mu h}((1-\alpha)+\alpha\gamma)2(1-\cos\theta) \end{bmatrix}}_{\mathbf{G}_{dr}} \times \begin{bmatrix} \widehat{U} \\ \widehat{P} \end{bmatrix} = \begin{bmatrix} 0 \\ 0 \end{bmatrix}. \tag{37}$$

Nontrivial solutions are obtained if $\det \mathbf{G}_{dr} = 0$, which provides the characteristic equation [62]. For the backward Euler scheme ($\alpha = 1$), the characteristic equation reduces to:

$$F_{dr}^{\alpha=1}(\gamma)=\left(\frac{K_{dr}}{M}+K_{dr}\frac{k_p\Delta t}{\mu h^2}2(1-\cos\theta)\right)\gamma^2+\left(-\frac{K_{dr}}{M}+b^2\right)\gamma-b^2=0. \tag{38}$$

The method is spectrally-stable if (i) $\max(|\gamma|)\leqslant 1$ for all values of θ, and (ii) $\gamma_1\neq\gamma_2$ when $\max(|\gamma|)=1$ [58]. From (38), the necessary and sufficient condition to hold spectral stability is

$$\tau\equiv\frac{b^2M}{K_{dr}}\leqslant 1, \tag{39}$$

where τ is the coupling strength between the flow and mechanics problems [30,59].

For the midpoint rule, $\alpha=0.5$, the characteristic equation reduces to:

$$\begin{aligned}F_{dr}^{\alpha=0.5}(\gamma)=&\left(\frac{1}{2}\frac{K_{dr}}{M}+\frac{K_{dr}}{2}\frac{k_p\Delta t}{\mu h^2}(1-\cos\theta)\right)\gamma^2\\&+\left(K_{dr}\frac{k_p\Delta t}{\mu h^2}(1-\cos\theta)+b^2\right)\gamma\\&-\left(\frac{1}{2}\frac{K_{dr}}{M}-\frac{K_{dr}}{2}\frac{k_p\Delta t}{\mu h^2}(1-\cos\theta)+b^2\right)=0,\end{aligned} \tag{40}$$

which yields $\max(|\gamma|)>1$, and we conclude that the drained split with the midpoint rule is unconditionally unstable.

Remark 1. For the backward Euler time discretization, $\alpha=1$, the stability condition is independent of time step size. This means that if the problem is such that $\tau>1$, stability of the drained split cannot be recovered by reducing the time step size. The von Neumann analysis also shows that one of the amplification factors is always negative, so the drained split will suffer from spurious oscillations [62].

Remark 2. Armero and Simo [30] use the backward Euler method for mechanics and the midpoint rule for flow, and the finite element method is used for both problems. This mixed time discretization yields the amplification factors:

$$\gamma=\begin{cases}1,\\ \frac{-b^2(1+\cos\theta)}{\frac{2K_{dr}}{3M}(2+\cos\theta)+\frac{k_p\Delta t}{\mu h^2}2(1-\cos\theta)},\end{cases} \tag{41}$$

from which the stability condition is $\tau\leqslant 1$, the same as in the backward Euler scheme with the mixed finite volume/finite element method. The stability condition (41) is sharper than the one in [30], obtained from a simple illustrative analysis with just two degrees of freedom:

$$2\frac{k_p\Delta tM}{\mu h^2}\geqslant\tau-\frac{4}{3}. \tag{42}$$

The mixed time discretization with the mixed finite volume/finite element method also yields the same stability criterion as the backward Euler time discretization.

5.2. Undrained split

The undrained split freezes the variation of fluid mass during the mechanical problem. From Eqs. (31) and (32), the pressure at element j at time $t_{n+\alpha}$ is

$$P_j^{n+\alpha}=P_j^n-\alpha bM(\varepsilon_v^{n+1}-\varepsilon_v^n), \tag{43}$$

where $\varepsilon_v^n=\left(U_{j+\frac{1}{2}}^n-U_{j-\frac{1}{2}}^n\right)/h$. Substituting Eq. (43) into Eq. (33), we obtain the discrete equations for the undrained split. Introducing a solution of the form Eqs. (35) and (36) into the discretized equations of the undrained split, we obtain the system of equations:

$$\underbrace{\begin{bmatrix}\left(\frac{K_{dr}}{h}((1-\alpha)+\alpha\gamma)\right.\\ \left.+\alpha\frac{b^2M}{h}(\gamma-1)\right)2(1-\cos\theta) & b2i\sin\frac{\theta}{2}\\ b(\gamma-1)2i\sin\frac{\theta}{2} & \frac{h}{M}(\gamma-1)\\ & +\frac{k_p\Delta t}{\mu h}((1-\alpha)+\alpha\gamma)2(1-\cos\theta)\end{bmatrix}}_{\boldsymbol{G}_{ud}}\times\begin{bmatrix}\widehat{U}\\ \widehat{P}\end{bmatrix}=\begin{bmatrix}0\\0\end{bmatrix}. \tag{44}$$

The characteristic equation $\det\boldsymbol{G}_{ud}=0$ reads:

$$\begin{aligned}F_{ud}^{\alpha}(\gamma)=&\left(\frac{K_{dr}}{M}\alpha+\alpha b^2+\left(K_{dr}+b^2M\right)\alpha^2\frac{k_p\Delta t}{\mu h^2}2(1-\cos\theta)\right)\gamma^2\\&+\left(\frac{K_{dr}}{M}(1-2\alpha)+\left(K_{dr}2(1-\alpha)+b^2M(1-2\alpha)\right)\right.\\&\left.\times\alpha\frac{k_p\Delta t}{\mu h^2}2(1-\cos\theta)+(1-2\alpha)b^2\right)\gamma\\&+\left(-\frac{K_{dr}}{M}(1-\alpha)-\left(\alpha b^2M-(1-\alpha)K_{dr}\right)\right.\\&\left.\times(1-\alpha)\frac{k_p\Delta t}{\mu h^2}2(1-\cos\theta)-(1-\alpha)b^2\right)=0,\end{aligned} \tag{45}$$

which yields $\max(|\gamma|)\leqslant 1$ when $0.5\leqslant\alpha\leqslant 1$. Therefore, the undrained split is unconditionally stable for $0.5\leqslant\alpha\leqslant 1$. This result extends to the nonlinear problem, as we will show in the next section.

Remark 3. When the backward Euler scheme is adopted for deformation and the midpoint rule is used for flow, the undrained split is also unconditionally stable.

6. Contractivity of the nonlinear continuum problem

In this section, we study the contractivity of the coupled continuum problem, and whether the dissipative structure of the coupled problem is inherited by the drained and undrained splits. The results of this section are not new, and they simply re-state the findings of Armero [26]. They are necessary, however, to set the stage for the algorithmic stability analysis of the next section.

Consider the following extension of the Biot equations of poroelasticity (Eqs. (5) and (6)) to the elastoplastic regime under isothermal conditions [5]:

$$\boldsymbol{\sigma}-\boldsymbol{\sigma}_0=\mathbf{C}_{dr}:(\boldsymbol{\varepsilon}-\boldsymbol{\varepsilon}_p)-b(p-p_0)\mathbf{1}, \tag{46}$$

$$\frac{1}{\rho_{f,0}}(m-m_0)-\phi_p=b(\varepsilon_v-\varepsilon_{p,v})+\frac{1}{M}(p-p_0), \tag{47}$$

where $\boldsymbol{\varepsilon}_p$ is the linearized plastic strain tensor, $\varepsilon_{p,v}=\operatorname{tr}\boldsymbol{\varepsilon}_p$, and ϕ_p is the plastic porosity. The elastic strain $\boldsymbol{\varepsilon}_e$ is defined as $\boldsymbol{\varepsilon}-\boldsymbol{\varepsilon}_p$, and $\varepsilon_{e,v}=\operatorname{tr}\boldsymbol{\varepsilon}_e$. The plastic porosity and plastic strain can be related to each other by assuming that $\dot{\phi}_p=\beta\dot{\varepsilon}_{p,v}$. Here, we further assume that $\beta=b$ [26], which yields:

$$\delta\phi_p=b\delta\varepsilon_{p,v}. \tag{48}$$

When the solid grains are incompressible, $\beta=b=1$.

The natural norm to show the dissipative character of the coupled problem is

$$\|\zeta\|_{\mathcal{T}}^2=\frac{1}{2}\int_\Omega\left(\boldsymbol{\sigma}':\mathbf{C}_{dr}^{-1}\boldsymbol{\sigma}'+\boldsymbol{\kappa}\cdot\boldsymbol{H}^{-1}\boldsymbol{\kappa}+\frac{1}{M}p^2\right)d\Omega, \tag{49}$$

$$\mathcal{T}:=\left\{\zeta\equiv(\boldsymbol{\sigma}',\boldsymbol{\kappa},p)\in\mathbb{S}\times\mathbb{R}^{n_{\text{int}}}\times\mathbb{R}:\sigma'_{ij}\in L^2(\Omega),\kappa_i\in L^2(\Omega),p\in L^2(\Omega)\right\}, \tag{50}$$

where σ'_{ij} and κ_i are the components of $\boldsymbol{\sigma}'$ and $\boldsymbol{\kappa}$, respectively, and $\boldsymbol{\kappa}$ is a vector of the stress-like plastic internal variables ("hardening

force"). n_{dim} is the dimension of the domain Ω, and n_{int} is the dimension of $\boldsymbol{\kappa}$. $\mathbb{S} = \mathbb{R}^{(n_{\text{dim}}+1)n_{\text{dim}}/2}$ is the vector space of symmetric rank-two tensors [64]. Note that the pressure can be discontinuous, and we only require the regularity $p \in L^2(\Omega)$. $\boldsymbol{H}$ is a positive-definite hardening modulus matrix, which relates changes in the internal stress variables $\boldsymbol{\kappa}$ with changes in the variables ξ:

$$\boldsymbol{\kappa} - \boldsymbol{\kappa}_0 = -\boldsymbol{H} \cdot \xi. \tag{51}$$

The vector $\boldsymbol{\xi}$ is a vector of the strain-like plastic internal variables [5]. The norm in Eq. (49) is motivated by the uncoupled mechanical and flow problems. The first and second terms correspond to the complementary Helmholtz free energy norm for the mechanical problem (albeit using the effective stress $\boldsymbol{\sigma}'$ instead of the total stress $\boldsymbol{\sigma}$), and the third term is the weighted L^2-norm in the flow problem [37].

We assume the material response follows an associated flow rule, or maximal plastic work (see Fig. 1). Such condition guarantees the following inequality [5]:

$$\int_\Omega \left((\boldsymbol{\pi}' - \boldsymbol{\sigma}') : \dot{\boldsymbol{\varepsilon}}_p + (\boldsymbol{\eta} - \boldsymbol{\kappa}) \cdot \dot{\boldsymbol{\xi}}\right) d\Omega \leqslant 0, \quad \forall (\boldsymbol{\pi}', \boldsymbol{\eta}) \in \mathcal{E}, \tag{52}$$

where $\boldsymbol{\pi}'$ and $\boldsymbol{\eta}$ are admissible (but otherwise arbitrary) effective stress and hardening force. The generalized elastic domain $\mathcal{E}$ is defined as:

$$\mathcal{E} := \{\boldsymbol{\Sigma} \equiv (\boldsymbol{\sigma}', \boldsymbol{\kappa}) \in \mathbb{S} \times \mathbb{R}^{n_{\text{int}}} : f_Y(\boldsymbol{\sigma}', \boldsymbol{\kappa}) \leqslant 0\}, \tag{53}$$

where $\boldsymbol{\Sigma}$ is a generalized effective stress. An admissible generalized effective stress is one that lies inside the elastic domain $\mathcal{E}$ or on its boundary $\partial\mathcal{E}$. We assume that the generalized elastic domain contains the origin $(\mathbf{0}, \mathbf{0})$, and that the yield surface f_Y is a convex function.

Let $\boldsymbol{\Sigma} \equiv (\boldsymbol{\sigma}', \boldsymbol{\kappa})$ and $\boldsymbol{\Pi} \equiv (\boldsymbol{\pi}', \boldsymbol{\eta})$ be generalized effective stresses. We define the bilinear form $\langle\!\langle \cdot, \cdot \rangle\!\rangle$:

$$\langle\!\langle \boldsymbol{\Sigma}, \boldsymbol{\Pi} \rangle\!\rangle := \int_\Omega \left(\boldsymbol{\sigma}' : \mathbf{C}_{dr}^{-1} \boldsymbol{\pi}' + \boldsymbol{\kappa} \cdot \boldsymbol{H}^{-1} \boldsymbol{\eta}\right) d\Omega, \tag{54}$$

and its associated norm $\|\cdot\|_{\mathcal{E}}$:

$$\|\boldsymbol{\Sigma}\|_{\mathcal{E}}^2 := \frac{1}{2} \langle\!\langle \boldsymbol{\Sigma}, \boldsymbol{\Sigma} \rangle\!\rangle. \tag{55}$$

To show contractivity of the coupled problem, let $(\boldsymbol{u}_0, p_0, \xi_0)$ and $(\tilde{\boldsymbol{u}}_0, \tilde{p}_0, \tilde{\xi}_0)$ be two arbitrary initial conditions, and denote by $(\boldsymbol{u}, p, \xi)$ and $(\tilde{\boldsymbol{u}}, \tilde{p}, \tilde{\xi})$ the corresponding solutions, which yield the remaining variables $(\boldsymbol{\sigma}', m, \boldsymbol{\kappa}, \boldsymbol{\varepsilon}_p)$ and $(\tilde{\boldsymbol{\sigma}}', \tilde{m}, \tilde{\boldsymbol{\kappa}}, \tilde{\boldsymbol{\varepsilon}}_p)$, respectively. By subtracting the two solutions, we obtain a solution to the problem with no source terms and with homogeneous boundary conditions, governed by the operator:

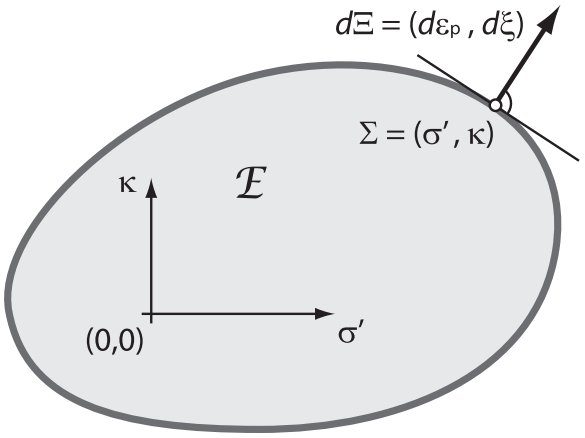

Fig. 1. Sketch of the generalized elastic domain $\mathcal{E}$. The thick gray line represents the yield surface $f_Y = 0$ on $\boldsymbol{\Sigma} \equiv (\boldsymbol{\sigma}', \boldsymbol{\kappa})$ generalized stress space. We assume an associated flow rule, so that the evolution of the generalized plastic–strain vector $d\boldsymbol{\Xi} \equiv (d\boldsymbol{\varepsilon}_p, d\boldsymbol{\xi})$ is colinear with $\nabla_{\boldsymbol{\Sigma}} f_Y$ at any point of the boundary $\partial\mathcal{E}$.

$$\begin{bmatrix} d\boldsymbol{u}^n \\ dp^n \end{bmatrix} \overset{\mathcal{A}_{fc}^0}{\to} \begin{bmatrix} d\boldsymbol{u}^{n+1} \\ dp^{n+1} \end{bmatrix}, \quad \text{where } \mathcal{A}_{fc}^0 : \begin{cases} \text{Div}\, d\boldsymbol{\sigma} = \mathbf{0}, \\ (\dot{dm}) + \text{Div}\, d\boldsymbol{w} = 0, \end{cases} \tag{56}$$

where $d(\cdot) = (\cdot) - (\tilde{\cdot})$ denotes the solution to the homogeneous problem. From Eqs. (46)–(48) and (51), we have:

$$d\boldsymbol{\sigma} = \mathbf{C}_{dr} : (d\boldsymbol{\varepsilon} - d\boldsymbol{\varepsilon}_p) - b\, dp \mathbf{1}, \tag{57}$$

$$\frac{dm}{\rho_{f,0}} = b\, d\varepsilon_v + \frac{1}{M} dp, \tag{58}$$

$$d\boldsymbol{\kappa} = -\boldsymbol{H} d\boldsymbol{\xi}. \tag{59}$$

From Eq. (52), we obtain

$$\int_\Omega \left((\tilde{\boldsymbol{\sigma}}' - \boldsymbol{\sigma}') : \dot{\boldsymbol{\varepsilon}}_p + (\tilde{\boldsymbol{\kappa}} - \boldsymbol{\kappa}) \cdot \dot{\boldsymbol{\xi}}\right) d\Omega \leqslant 0, \quad \text{choosing } (\boldsymbol{\pi}', \boldsymbol{\eta}) = (\tilde{\boldsymbol{\sigma}}', \tilde{\boldsymbol{\kappa}}), \tag{60}$$

$$\int_\Omega \left((\boldsymbol{\sigma}' - \tilde{\boldsymbol{\sigma}}') : \dot{\tilde{\boldsymbol{\varepsilon}}}_p + (\boldsymbol{\kappa} - \tilde{\boldsymbol{\kappa}}) \cdot \dot{\tilde{\boldsymbol{\xi}}}\right) d\Omega \leqslant 0, \quad \text{choosing } (\boldsymbol{\pi}', \boldsymbol{\eta}) = (\boldsymbol{\sigma}', \boldsymbol{\kappa}). \tag{61}$$

Adding Eqs. (60) and (61), we arrive at the non-negativity of the rate of plastic dissipation:

$$D_p^d := \int_\Omega \left(d\boldsymbol{\sigma}' : d\dot{\boldsymbol{\varepsilon}}_p + d\boldsymbol{\kappa} \cdot \dot{d\boldsymbol{\xi}}\right) d\Omega \geqslant 0. \tag{62}$$

Then we obtain, from Eq. (49):

$$\begin{aligned} \|d\zeta\|_{\mathcal{T}}^2 &= \frac{1}{2} \int_\Omega \left(d\boldsymbol{\sigma}' : \mathbf{C}_{dr}^{-1} d\boldsymbol{\sigma}' + d\boldsymbol{\kappa} \cdot \boldsymbol{H}^{-1} d\boldsymbol{\kappa} + \frac{1}{M} dp^2\right) d\Omega, \\ &= \frac{1}{2} \int_\Omega \left(d\boldsymbol{\varepsilon}_e : \mathbf{C}_{dr} d\boldsymbol{\varepsilon}_e + d\boldsymbol{\xi} \cdot \boldsymbol{H} d\boldsymbol{\xi} + M \left(\frac{dm_e}{\rho_{f,0}} - b d\varepsilon_{e,v}\right)^2\right) d\Omega, \\ &= \|d\boldsymbol{\chi}\|_{\mathcal{N}}^2, \end{aligned} \tag{63}$$

where we define the norm:

$$\|\boldsymbol{\chi}\|_{\mathcal{N}}^2 = \frac{1}{2} \int_\Omega \left(\boldsymbol{\varepsilon}_e : \mathbf{C}_{dr} \boldsymbol{\varepsilon}_e + \boldsymbol{\xi} \cdot \boldsymbol{H} \boldsymbol{\xi} + M \left(\frac{m_e}{\rho_{f,0}} - b \varepsilon_{e,v}\right)^2\right) d\Omega, \tag{64}$$

$$\mathcal{N} := \left\{\boldsymbol{\chi} \equiv (\boldsymbol{\varepsilon}_e, \boldsymbol{\xi}, m_e) \in \mathbb{S} \times \mathbb{R}^{n_{\text{int}}} \times \mathbb{R} : \varepsilon_{e,ij} \in L^2(\Omega),\, \xi_i \in L^2(\Omega), m_e \in L^2(\Omega)\right\}, \tag{65}$$

where $\varepsilon_{e,ij}$ and ξ_i are the components of $\boldsymbol{\varepsilon}_e$ and $\boldsymbol{\xi}$, respectively. The definition of the natural norm in Eq. (64) originates from the Helmholtz free energy of the system [5].

Let us denote $\|d\boldsymbol{\chi}\|_{\mathcal{N}}^2$ by Ψ^d, for convenience. Then, the coupled problem enjoys the following contractivity property,

$$\begin{aligned} \frac{d\Psi^d}{dt} &= \frac{\partial \Psi^d}{\partial d\boldsymbol{\varepsilon}_e} : d\dot{\boldsymbol{\varepsilon}}_e + \frac{\partial \Psi^d}{\partial d\boldsymbol{\chi}} \cdot \dot{d\boldsymbol{\xi}} + \frac{\partial \Psi^d}{\partial dm_e} \dot{dm}_e \\ &= \int_\Omega \left(d\boldsymbol{\sigma}' : d\dot{\boldsymbol{\varepsilon}}_e - M \left(\frac{dm_e}{\rho_{f,0}} - b d\varepsilon_{e,v}\right) b d\dot{\varepsilon}_{e,v} - d\boldsymbol{\kappa} \cdot \dot{d\boldsymbol{\xi}} + \left(\frac{dm_e}{\rho_{f,0}} - b d\varepsilon_{e,v}\right) \dot{dm}_e\right) d\Omega \\ &= \int_\Omega \left(d\boldsymbol{\sigma} : d\dot{\boldsymbol{\varepsilon}} + \frac{dp}{\rho_{f,0}} \dot{dm}\right) d\Omega - \underbrace{\int_\Omega \left(d\boldsymbol{\sigma}' : d\dot{\boldsymbol{\varepsilon}}_p + d\boldsymbol{\kappa} \cdot \dot{d\boldsymbol{\xi}}\right) d\Omega}_{D_p^d} \\ &= \int_\Omega \left(d\boldsymbol{\sigma} : d\dot{\boldsymbol{\epsilon}} - dp \text{Div}(d\boldsymbol{v})\right) d\Omega - D_p^d \quad (\text{from Eq. } (56)_2) \\ &= -\int_\Omega (dp \text{Div}(d\boldsymbol{v})) d\Omega - D_p^d \quad (\text{since } \int_\Omega d\boldsymbol{\sigma} : d\dot{\boldsymbol{\varepsilon}} d\Omega = 0 \quad \text{from Eq. } (56)_1) \\ &= -\int_\Omega d\boldsymbol{v} \cdot \mu \boldsymbol{k}^{-1} d\boldsymbol{v} d\Omega - D_p^d \quad (\text{from Eq. } (15), \text{ with } \boldsymbol{v} \in H(\text{div}, \Omega)) \\ &\leqslant 0 \quad (\text{from Eq. } (62)). \end{aligned} \tag{66}$$

Eq. (66) implies:

$$\|\boldsymbol{\chi}(t) - \tilde{\boldsymbol{\chi}}(t)\|_{\mathcal{N}} \leqslant \|\boldsymbol{\chi}_0 - \tilde{\boldsymbol{\chi}}_0\|_{\mathcal{N}}, \tag{67}$$

from which it follows that the coupled problem is contractive with respect to the norm $\|\cdot\|_{\mathcal{N}}$. Thus, the norms in Eqs. (49) and (64) are the appropriate norms to show contractivity, which is equivalent to thermodynamic stability and uniqueness of the solution [5]. To be precise, stability of the displacement field requires a bounded plastic strain, which in turn requires the strict inequality $\|\boldsymbol{H}\| > 0$. Therefore, perfect plasticity ($\|\boldsymbol{H}\| = 0$) does not guarantee stability of the displacement field Simo [37].

We now analyze whether the drained and undrained splits are contractive.

6.1. Drained split

Introducing two arbitrary initial conditions and taking similar steps to the fully coupled method, the drained split for the problem with no source terms and homogeneous boundary conditions reads:

$$\begin{bmatrix} d\boldsymbol{u}^n \\ dp^n \end{bmatrix} \overset{\mathcal{A}^{0,u}_{dr}}{\rightarrow} \begin{bmatrix} d\boldsymbol{u}^{n+1} \\ dp^n \end{bmatrix} \overset{\mathcal{A}^{0,p}_{dr}}{\rightarrow} \begin{bmatrix} d\boldsymbol{u}^{n+1} \\ dp^{n+1} \end{bmatrix},$$
$$\text{where } \begin{cases} \mathcal{A}^{0,u}_{dr} : \mathrm{Div}\, d\boldsymbol{\sigma} = \boldsymbol{0},\ \delta dp = 0, \\ \mathcal{A}^{0,p}_{dr} : d\dot{m} + \mathrm{Div}\, d\boldsymbol{w} = 0,\ \delta d\boldsymbol{\varepsilon} = \boldsymbol{0},\ \delta d\boldsymbol{\varepsilon}_p = \boldsymbol{0},\ \delta d\xi = \boldsymbol{0}. \end{cases} \tag{68}$$

For the flow step:

$$\left.\frac{d\Psi^d}{dt}\right|_{\mathcal{A}^{0,p}_{dr}} = \int_\Omega \left(d\boldsymbol{\sigma} : d\dot{\epsilon} + \frac{dp}{\rho_{f,0}} d\dot{m} \right) d\Omega - \underbrace{\int_\Omega \left(d\boldsymbol{\sigma}' : d\dot{\boldsymbol{\varepsilon}}_p + d\boldsymbol{\kappa} \cdot d\dot{\xi} \right) d\Omega}_{D^d_p}$$
$$= -\int_\Omega dp\, \mathrm{Div}(d\boldsymbol{v})\, d\Omega \quad (\text{since } \delta d\boldsymbol{\varepsilon} = \boldsymbol{0}, \delta d\boldsymbol{\varepsilon}_p = \boldsymbol{0}, \delta d\xi = \boldsymbol{0})$$
$$= -\int_\Omega d\boldsymbol{v} \cdot \mu \boldsymbol{k}^{-1} d\boldsymbol{v}\, d\Omega \leqslant 0. \tag{69}$$

For the mechanics step:

$$\left.\frac{d\Psi^d}{dt}\right|_{\mathcal{A}^{0,u}_{dr}} = \int_\Omega \left(d\boldsymbol{\sigma} : d\dot{\epsilon} + \frac{dp}{\rho_{f,0}} d\dot{m} \right) d\Omega - \underbrace{\int_\Omega \left(d\boldsymbol{\sigma}' : d\dot{\boldsymbol{\varepsilon}}_p + d\boldsymbol{\kappa} \cdot d\dot{\xi} \right) d\Omega}_{D^d_p}$$
$$= \int_\Omega \left(d\boldsymbol{\sigma} : d\dot{\epsilon} + \frac{dp}{\rho_{f,0}} b d\dot{\epsilon}_v \right) d\Omega - D^d_p \quad (\text{since } \delta dp = 0)$$
$$= \int_\Omega \frac{dp}{\rho_{f,0}} b d\dot{\epsilon}_v\, d\Omega - D^d_p \quad (\text{since } \mathrm{Div}\, d\boldsymbol{\sigma} = \boldsymbol{0}) \not\leqslant 0. \tag{70}$$

From the expression above, one cannot guarantee that the natural norm of the solution decreases during the mechanics step. Therefore, the drained split method does not inherit the contractive character of the continuum coupled problem. This has been pointed out by Armero [26].

6.2. Undrained split

Following the same procedure as above, that is, introducing two arbitrary initial conditions and subtracting the corresponding solutions, the undrained split for the difference is given by

$$\begin{bmatrix} d\boldsymbol{u}^n \\ dp^n \end{bmatrix} \overset{\mathcal{A}^{0,u}_{ud}}{\rightarrow} \begin{bmatrix} d\boldsymbol{u}^{n+1} \\ dp^* \end{bmatrix} \overset{\mathcal{A}^{0,p}_{ud}}{\rightarrow} \begin{bmatrix} d\boldsymbol{u}^{n+1} \\ dp^{n+1} \end{bmatrix},$$
$$\text{where } \begin{cases} \mathcal{A}^{0,u}_{ud} : \mathrm{Div}\, d\boldsymbol{\sigma} = \boldsymbol{0},\ \delta dm = 0, \\ \mathcal{A}^{0,p}_{ud} : d\dot{m} + \mathrm{Div}\, d\boldsymbol{w} = 0,\ \delta d\boldsymbol{\varepsilon} = \boldsymbol{0},\ \delta d\boldsymbol{\varepsilon}_p = \boldsymbol{0},\ \delta d\xi = \boldsymbol{0}. \end{cases} \tag{71}$$

The contractivity properties of the flow step are the same as for the drained split. In contrast, for the mechanics step we have:

$$\left.\frac{d\Psi^d}{dt}\right|_{\mathcal{A}^{0,u}_{ud}} = \int_\Omega \left(d\boldsymbol{\sigma} : d\dot{\epsilon} + \frac{dp}{\rho_{f,0}} d\dot{m} \right) d\Omega - \underbrace{\int_\Omega \left(d\boldsymbol{\sigma}' : d\dot{\boldsymbol{\varepsilon}}_p + d\boldsymbol{\kappa} \cdot d\dot{\xi} \right) d\Omega}_{D^d_p}$$
$$= \int_\Omega d\boldsymbol{\sigma} : d\dot{\epsilon}\, d\Omega - D^d_p \quad (\text{since } \delta dm = 0)$$
$$= -D^d_p \quad (\text{since } \mathrm{Div}\, \boldsymbol{\sigma} = \boldsymbol{0}) \leqslant 0. \tag{72}$$

Therefore, the undrained split satisfies the contractivity property of the continuum problem, which is equivalent to its dissipative character [26].

7. Algorithmic stability of the nonlinear problem

The analysis of the previous section confirms that the undrained split inherits the contractivity property (that is, the dissipative character [26]) of the continuum problem. In this section we study what time-integration schemes are B-stable [65]. By B-stability we mean the algorithmic counterpart of contractivity [37,48,66], i.e.,

$$\|d\boldsymbol{\chi}^{n+1}\|^2_{\mathcal{N}} \leqslant \|d\boldsymbol{\chi}^n\|^2_{\mathcal{N}} \quad \forall n, \tag{73}$$

where $d\boldsymbol{\chi}$ is the difference between two solutions with different initial conditions, and n and $n+1$ refer to two consecutive time steps.

Since the drained split does not honor the dissipative character, it clearly cannot provide an unconditionally stable algorithm. Thus, we focus exclusively on the *undrained split*. Our analysis follows that of Simo [37], and Simo and Govindjee [48] for elastoplasticity, and that of Simo [37] for the nonlinear heat equation. We extend their results to the coupled problem.

7.1. The mechanics step

We solve the mechanical problem first by means of the return mapping algorithm [67,68], for which we adopt the generalized midpoint rule [37,48]. The algorithmic counterpart of Eq. (52) is

$$\langle\!\langle \boldsymbol{\Sigma}^{tr,n+\alpha} - \boldsymbol{\Sigma}^{n+\alpha}, \boldsymbol{\Pi} - \boldsymbol{\Sigma}^{n+\alpha} \rangle\!\rangle \leqslant 0 \quad \forall \boldsymbol{\Pi} \in \mathcal{E}, \tag{74}$$

where $\boldsymbol{\Sigma} = (\boldsymbol{\sigma}', \boldsymbol{\kappa})$ is a generalized effective stress which is constrained to lie within the elastic domain $\mathcal{E}$, $\boldsymbol{\Pi} = (\boldsymbol{\pi}', \boldsymbol{\eta})$ is another generalized effective stress, and $\boldsymbol{\Sigma}^{tr,n+\alpha}$ from the elastic trial step is defined as $(\boldsymbol{\sigma}'^n + \alpha \mathbf{C}_{dr}\, \Delta\boldsymbol{\varepsilon}^n, \boldsymbol{\kappa}^n)$. In what follows, we denote by $\Delta(\cdot)^n \equiv (\cdot)^{n+1} - (\cdot)^n$. Fig. 2 shows the geometric interpretation of Eq. (74).

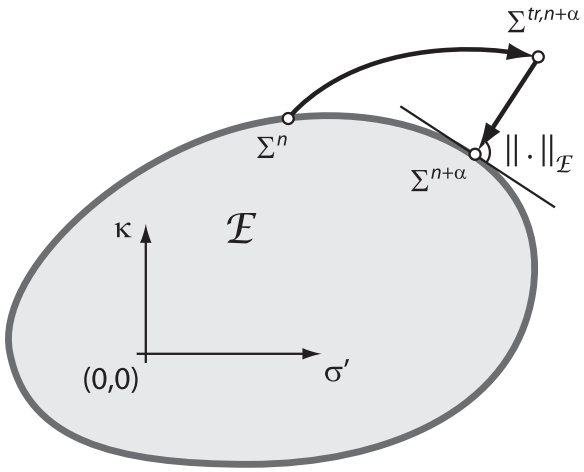

Fig. 2. Geometric interpretation of the return mapping algorithm in effective stress space (modified from [66]).

Let $(\boldsymbol{u}^n, p^n, \xi^n)$ and $(\tilde{\boldsymbol{u}}^n, \tilde{p}^n, \tilde{\xi}^n)$ be two arbitrary solutions at time t_n, with the associated variables $(\boldsymbol{\sigma}'^n, m^n, \boldsymbol{\kappa}^n, \boldsymbol{\varepsilon}_p^n)$ and $(\tilde{\boldsymbol{\sigma}}'^n, \tilde{m}^n, \tilde{\boldsymbol{\kappa}}^n, \tilde{\boldsymbol{\varepsilon}}_p^n)$, respectively. Then, discretization of Eq. $(71)_1$ with the generalized midpoint rule yields:

$$\mathrm{Div}\, d\boldsymbol{\sigma}^{n+\alpha} = \boldsymbol{0}, \quad \Delta dm = 0, \tag{75}$$

where $d\boldsymbol{\sigma}^{n+\alpha} = \boldsymbol{\sigma}^{n+\alpha} - \tilde{\boldsymbol{\sigma}}^{n+\alpha}$. From Eq. (74),

$$\langle\!\langle \boldsymbol{\Sigma}^{tr,n+\alpha} - \boldsymbol{\Sigma}^{n+\alpha}, \tilde{\boldsymbol{\Sigma}}^{n+\alpha} - \boldsymbol{\Sigma}^{n+\alpha} \rangle\!\rangle \leqslant 0 \quad (\text{choosing } \boldsymbol{\Pi} = \tilde{\boldsymbol{\Sigma}}^{n+\alpha}), \tag{76}$$

$$\langle\!\langle \tilde{\boldsymbol{\Sigma}}^{tr,n+\alpha} - \tilde{\boldsymbol{\Sigma}}^{n+\alpha}, \boldsymbol{\Sigma}^{n+\alpha} - \tilde{\boldsymbol{\Sigma}}^{n+\alpha} \rangle\!\rangle \leqslant 0 \quad (\text{choosing } \boldsymbol{\Pi} = \boldsymbol{\Sigma}^{n+\alpha}). \tag{77}$$

Adding Eqs. (76) and (77):

$$\langle\!\langle d\boldsymbol{\Sigma}^n - d\boldsymbol{\Sigma}^{n+\alpha}, -d\boldsymbol{\Sigma}^{n+\alpha} \rangle\!\rangle + \langle\!\langle (\alpha \mathbf{C}_{dr} \Delta d\boldsymbol{\varepsilon}^n, \boldsymbol{0}), (-d\boldsymbol{\sigma}'^{n+\alpha}, -d\boldsymbol{\kappa}^{n+\alpha}) \rangle\!\rangle \leqslant 0. \tag{78}$$

The first term of Eq. (78) can be written as:

$$\begin{aligned}
\langle\!\langle d\boldsymbol{\Sigma}^n - d\boldsymbol{\Sigma}^{n+\alpha}, -d\boldsymbol{\Sigma}^{n+\alpha} \rangle\!\rangle &= -\langle\!\langle \alpha(d\boldsymbol{\Sigma}^n - d\boldsymbol{\Sigma}^{n+1}), d\boldsymbol{\Sigma}^{n+1/2} \\
&\quad + \left(\alpha - \frac{1}{2}\right)(d\boldsymbol{\Sigma}^{n+1} - d\boldsymbol{\Sigma}^n) \rangle\!\rangle \\
&= \alpha\left(\|d\boldsymbol{\Sigma}^{n+1}\|_{\mathcal{E}}^2 - \|d\boldsymbol{\Sigma}^n\|_{\mathcal{E}}^2 \right) \\
&\quad + \alpha(2\alpha - 1)\|d\boldsymbol{\Sigma}^{n+1} - d\boldsymbol{\Sigma}^n\|_{\mathcal{E}}^2,
\end{aligned} \tag{79}$$

where $\boldsymbol{\Sigma}^{n+1/2} = 1/2(\boldsymbol{\Sigma}^n + \boldsymbol{\Sigma}^{n+1})$. The second term of Eq. (78) can be written as:

$$\begin{aligned}
&\langle\!\langle (\alpha \mathbf{C}_{dr} \Delta d\boldsymbol{\varepsilon}^n, \boldsymbol{0}), (-d\boldsymbol{\sigma}'^{n+\alpha}, -d\boldsymbol{\kappa}^{n+\alpha}) \rangle\!\rangle \\
&\quad = -\int_\Omega \alpha \Delta d\boldsymbol{\varepsilon}^n : d\boldsymbol{\sigma}'^{n+\alpha}\, d\Omega \\
&\quad = -\alpha \int_\Omega \Delta d\boldsymbol{\varepsilon}^n : (d\boldsymbol{\sigma}^{n+\alpha} + b dp^{n+\alpha}\mathbf{1})\, d\Omega \\
&\quad = -\alpha \int_\Omega \Delta d\boldsymbol{\varepsilon}^n : b dp^{n+\alpha}\mathbf{1}\, d\Omega \quad (\text{from Eq. (75)}) \\
&\quad = \alpha \int_\Omega \frac{1}{M}(dp^{n+1} - dp^n) dp^{n+\alpha}\, d\Omega \quad (\text{from Eq. (6) and } \Delta dm = 0) \\
&\quad = \alpha \frac{1}{2M}\left(\|dp^{n+1}\|_{L^2}^2 - \|dp^n\|_{L^2}^2 \right) + \alpha(2\alpha - 1)\frac{1}{2M}\|dp^{n+1} - dp^n\|_{L^2}^2.
\end{aligned} \tag{80}$$

Substituting Eqs. (79) and (80) into Eq. (78):

$$\begin{aligned}
&\alpha\left(\|d\boldsymbol{\Sigma}^{n+1}\|_{\mathcal{E}}^2 - \|d\boldsymbol{\Sigma}^n\|_{\mathcal{E}}^2 + \frac{1}{2M}\left(\|dp^{n+1}\|_{L^2}^2 - \|dp^n\|_{L^2}^2 \right) \right) \\
&\quad + \alpha(2\alpha - 1)\left(\|d\boldsymbol{\Sigma}^{n+1} - d\boldsymbol{\Sigma}^n\|_{\mathcal{E}}^2 + \frac{1}{2M}\|dp^{n+1} - dp^n\|_{L^2}^2 \right) \leqslant 0.
\end{aligned} \tag{81}$$

Then, the evolution of the norm at the discrete time level during the solution of the mechanics step is

$$\begin{aligned}
&\|d\boldsymbol{\chi}^{n+1}\|_{\mathcal{N}}^2 - \|d\boldsymbol{\chi}^n\|_{\mathcal{N}}^2 \\
&\quad = \|d\zeta^{n+1}\|_{\mathcal{T}}^2 - \|d\zeta^n\|_{\mathcal{T}}^2 \\
&\quad = \|d\boldsymbol{\Sigma}^{n+1}\|_{\mathcal{E}}^2 + \frac{1}{2M}\|dp^{n+1}\|_{L^2}^2 - \|d\boldsymbol{\Sigma}^n\|_{\mathcal{E}}^2 - \frac{1}{2M}\|dp^n\|_{L^2}^2 \\
&\qquad (\text{from Eqs. (49), (54) and (55)}) \\
&\quad \leqslant -(2\alpha - 1)\left(\|d\boldsymbol{\Sigma}^{n+1} - d\boldsymbol{\Sigma}^n\|_{\mathcal{E}}^2 + \frac{1}{2M}\|dp^{n+1} - dp^n\|_{L^2}^2 \right) \quad (\text{from (81)}).
\end{aligned} \tag{82}$$

The B-stability condition (73) is satisfied during the mechanical step if $0.5 \leqslant \alpha \leqslant 1$.

Remark 4. This result generalizes the analysis of Simo [37] to coupled poroelastoplasticity. In the uncoupled problem, Eq. (80) is identically zero, and the natural norm does not include a contribution from the pore fluid pressure.

7.2. The flow step

The second step in the sequential scheme is to solve the flow problem. Since all the mechanical variables (deformation and stress) are frozen during the flow step, the problem reduces to the heat conduction equation, and the nonlinear stability analysis is standard [69,37]. We summarize it here for completeness.

After time discretization with the generalized midpoint rule, Eq. $(71)_2$ leads to:

$$\begin{aligned}
&\frac{1}{M}\frac{dp^{n+1} - dp^n}{\Delta t} + \mathrm{Div}\, d\boldsymbol{v}^{n+\alpha} = 0, \quad \text{with } \Delta d\boldsymbol{\varepsilon} = \boldsymbol{0}, \\
&\Delta d\boldsymbol{\varepsilon}_p = \boldsymbol{0}, \quad \Delta d\boldsymbol{\xi} = \boldsymbol{0}.
\end{aligned} \tag{83}$$

Multiplying by $dp^{n+\alpha}$, integrating over the domain Ω, and using the divergence theorem, we obtain:

$$\begin{aligned}
\int_\Omega dp^{n+\alpha}\frac{1}{M}\frac{dp^{n+1} - dp^n}{\Delta t}\, d\Omega &= \int_\Omega \mathbf{Grad}\, dp^{n+\alpha} \cdot d\boldsymbol{v}^{n+\alpha}\, d\Omega \\
&= -\int_\Omega d\boldsymbol{v}^{n+\alpha} \cdot \mu \boldsymbol{k}^{-1} d\boldsymbol{v}^{n+\alpha}\, d\Omega \\
&\qquad (\text{from Darcy's law}).
\end{aligned} \tag{84}$$

From Eq. (83):

$$\|d\boldsymbol{\Sigma}^{n+1}\|_{\mathcal{E}}^2 = \|d\boldsymbol{\Sigma}^n\|_{\mathcal{E}}^2. \tag{85}$$

Using Eq. (85) and the following identity:

$$\begin{aligned}
&\int_\Omega dp^{n+\alpha}\frac{1}{M}\left(dp^{n+1} - dp^n\right) d\Omega \\
&\quad = \frac{1}{2M}\left(\|dp^{n+1}\|_{L^2}^2 - \|dp^n\|_{L^2}^2 \right) + (2\alpha - 1)\frac{1}{2M}\|dp^{n+1} - dp^n\|_{L^2}^2,
\end{aligned} \tag{86}$$

the evolution of the norm during the flow step is

$$\begin{aligned}
\|d\boldsymbol{\chi}^{n+1}\|_{\mathcal{N}}^2 - \|d\boldsymbol{\chi}^n\|_{\mathcal{N}}^2 &= \|d\zeta^{n+1}\|_{\mathcal{T}}^2 - \|d\zeta^n\|_{\mathcal{T}}^2 \\
&= \frac{1}{2M}\left(\|dp^{n+1}\|_{L^2}^2 - \|dp^n\|_{L^2}^2 \right) \\
&= -(2\alpha - 1)\frac{1}{2M}\|dp^{n+1} - dp^n\|_{L^2}^2 \\
&\quad - \Delta t \int_\Omega d\boldsymbol{v}^{n+\alpha} \cdot \mu \boldsymbol{k}^{-1} d\boldsymbol{v}^{n+\alpha}\, d\Omega.
\end{aligned} \tag{87}$$

The B-stability condition (73) is satisfied during the flow step if $0.5 \leqslant \alpha \leqslant 1$. The stability condition during the flow step is identical to the uncoupled problem, where the proper norm to show stability is a weighted L^2 norm of the pressure [69,37]. From Eqs. (82) and (87), the condition for B-stability of the undrained split is $0.5 \leqslant \alpha \leqslant 1$. Moreover, since this condition is obtained independently for the mechanics and flow steps, we infer that the undrained split is B-stable for *mixed* time discretizations based on a generalized midpoint rule for each subproblem, with $\alpha_{\mathrm{mech}} \neq \alpha_{\mathrm{flow}}$, as long as $0.5 \leqslant \alpha_{\mathrm{mech}} \leqslant 1$ and $0.5 \leqslant \alpha_{\mathrm{flow}} \leqslant 1$.

8. Error estimation

We now investigate convergence of the drained and undrained splits. For simplicity, we consider the linear problem only. We employ the matrix algebra and spectral methods to analyze the behavior of the error as a function of the number of iterations.

8.1. Error estimation of the drained split by matrix algebra

For a sequential solution strategy, we can write:

$$\left\|\mathbf{e}_{ts}^{n+1,n_{\text{iter}}}\right\| \leqslant \left\|\mathbf{x}_t^{n+1}-\mathbf{x}_f^{n+1}\right\| + \left\|\mathbf{x}_f^{n+1}-\mathbf{x}_s^{n+1,n_{\text{iter}}}\right\| = \mathbf{O}(\Delta t) + \left\|\mathbf{x}_f^{n+1}-\mathbf{x}_s^{n+1,n_{\text{iter}}}\right\|, \tag{88}$$

where $\mathbf{e}_{ts}$ is the error between the true solution and the numerical solutions from the sequential method, and $\|\cdot\|$ is an appropriate norm (e.g., L^2 norm), $\mathbf{e}_{fs}^{n+1}=\mathbf{x}_f^{n+1}-\mathbf{x}_s^{n+1,n_{\text{iter}}}$ is the error between the fully coupled and sequential methods, n is the time step, n_{iter} is the iteration number within a time step, and $\mathbf{x}^t=[\mathbf{u}^t,\mathbf{p}^t]$ denotes the displacement–pressure solution to the coupled problem. The subscripts f and s (i.e., $(\cdot)_f$ and $(\cdot)_s$) denote the fully coupled and sequential methods, respectively, and the subscript t (i.e., $(\cdot)_t$) denotes the true solution. If $\|\mathbf{e}_{fs}\|=O(\Delta t^m)$, where $m>0$, the numerical scheme is convergent [62], whereas if $\|\mathbf{e}_{fs}\|=O(1)$, the numerical scheme is not convergent. Turska and Schrefler [70] show that $\|\mathbf{x}_t^{n+1}-\mathbf{x}_f^{n+1}\|=O(\Delta t)$ when the backward Euler time discretization is employed.

For the fully coupled method, the algebraic form of the coupled problem is

$$\underbrace{\begin{bmatrix}\mathbf{K} & -\mathbf{L}^t\\ \mathbf{L} & \mathbf{F}\end{bmatrix}}_{\mathbf{A}}\begin{bmatrix}\mathbf{u}\\ \mathbf{p}\end{bmatrix}^{n+1} - \underbrace{\begin{bmatrix}\mathbf{0} & \mathbf{0}\\ \mathbf{L} & \mathbf{Q}\end{bmatrix}}_{\mathbf{B}}\begin{bmatrix}\mathbf{u}\\ \mathbf{p}\end{bmatrix}^{n} = \underbrace{\begin{bmatrix}\mathbf{f}_{\mathbf{u}}\\ \mathbf{f}_{\mathbf{p}}\end{bmatrix}^{n+1}}_{\mathbf{f}}, \tag{89}$$

where $\mathbf{K}$ is the stiffness matrix from the drained moduli, and $\mathbf{F}=\mathbf{Q}+\Delta t\mathbf{T}$ [25]. $\mathbf{Q}$ and $\mathbf{T}$ are the fluid compressibility matrix, which includes the Biot modulus, and the transmissibility matrix of the flow problem, respectively. $\mathbf{L}$ is associated with the coupling coefficient, the Biot coefficient. The drained split decomposes matrix $\mathbf{A}$ into:

$$\begin{bmatrix}\mathbf{K} & \mathbf{0}\\ \mathbf{L} & \mathbf{F}\end{bmatrix}\begin{bmatrix}\mathbf{u}\\ \mathbf{p}\end{bmatrix}^{n+1,k+1} - \begin{bmatrix}\mathbf{0} & \mathbf{L}^t\\ \mathbf{0} & \mathbf{0}\end{bmatrix}\begin{bmatrix}\mathbf{u}\\ \mathbf{p}\end{bmatrix}^{n+1,k} - \begin{bmatrix}\mathbf{0} & \mathbf{0}\\ \mathbf{L} & \mathbf{Q}\end{bmatrix}\begin{bmatrix}\mathbf{u}\\ \mathbf{p}\end{bmatrix}^{n} = \begin{bmatrix}\mathbf{f}_{\mathbf{u}}\\ \mathbf{f}_{\mathbf{p}}\end{bmatrix}^{n+1}, \tag{90}$$

where k is the iteration index. From Eqs. (89) and (90), the errors of pressure and displacement between the fully coupled method and drained split are:

$$\begin{aligned}\begin{bmatrix}\mathbf{e}_{fs,\mathbf{u}}\\ \mathbf{e}_{fs,\mathbf{p}}\end{bmatrix}^{n+1,k+1} &= \begin{bmatrix}\mathbf{K} & \mathbf{0}\\ \mathbf{L} & \mathbf{F}\end{bmatrix}^{-1}\left(\begin{bmatrix}\mathbf{0} & \mathbf{L}^t\\ \mathbf{0} & \mathbf{0}\end{bmatrix}\begin{bmatrix}\mathbf{e}_{fs,\mathbf{u}}\\ \mathbf{e}_{fs,\mathbf{p}}\end{bmatrix}^{n+1,k} + \begin{bmatrix}\mathbf{0} & \mathbf{0}\\ \mathbf{L} & \mathbf{Q}\end{bmatrix}\begin{bmatrix}\mathbf{e}_{fs,\mathbf{u}}\\ \mathbf{e}_{fs,\mathbf{p}}\end{bmatrix}^{n}\right)\\ &= \begin{bmatrix}\mathbf{K}^{-1} & \mathbf{0}\\ -\mathbf{F}^{-1}\mathbf{L}\mathbf{K}^{-1} & \mathbf{F}^{-1}\end{bmatrix}\\ &\quad\times\left(\begin{bmatrix}\mathbf{0} & \mathbf{L}^t\\ \mathbf{0} & \mathbf{0}\end{bmatrix}\begin{bmatrix}\mathbf{e}_{fs,\mathbf{u}}\\ \mathbf{e}_{fs,\mathbf{p}}\end{bmatrix}^{n+1,k} + \begin{bmatrix}\mathbf{0} & \mathbf{0}\\ \mathbf{L} & \mathbf{Q}\end{bmatrix}\begin{bmatrix}\mathbf{e}_{fs,\mathbf{u}}\\ \mathbf{e}_{fs,\mathbf{p}}\end{bmatrix}^{n}\right)\\ &= \underbrace{\begin{bmatrix}\mathbf{0} & \mathbf{K}^{-1}\mathbf{L}^t\\ \mathbf{0} & -\mathbf{F}^{-1}\mathbf{L}\mathbf{K}^{-1}\mathbf{L}^t\end{bmatrix}}_{\mathbf{D}}\begin{bmatrix}\mathbf{e}_{fs,\mathbf{u}}\\ \mathbf{e}_{fs,\mathbf{p}}\end{bmatrix}^{n+1,k}\\ &\quad+\underbrace{\begin{bmatrix}\mathbf{0} & \mathbf{0}\\ \mathbf{F}^{-1}\mathbf{L} & \mathbf{F}^{-1}\mathbf{Q}\end{bmatrix}}_{\mathbf{H}}\begin{bmatrix}\mathbf{e}_{fs,\mathbf{u}}\\ \mathbf{e}_{fs,\mathbf{p}}\end{bmatrix}^{n},\end{aligned} \tag{91}$$

where $\mathbf{e}_{fs}=\begin{bmatrix}\mathbf{e}_{fs,\mathbf{u}}\\ \mathbf{e}_{fs,\mathbf{p}}\end{bmatrix}$, and $\mathbf{e}_{fs}^{n}=\mathbf{e}_{fs}^{n,n_{\text{iter}}}$. Then:

$$\begin{aligned}\mathbf{e}_{fs}^{n+1,n_{\text{iter}}} &= \mathbf{D}^{n_{\text{iter}}}\mathbf{e}^{n+1,0}+\sum_{l=1}^{n_{\text{iter}}}\mathbf{D}^{l-1}\mathbf{H}\mathbf{e}_{fs}^{n,n_{\text{iter}}}\\ &= \mathbf{D}^{n_{\text{iter}}}\left(\mathbf{x}_f^{n+1}-\mathbf{x}_f^{n}\right)+\underbrace{\left(\mathbf{D}^{n_{\text{iter}}}+\sum_{l=1}^{n_{\text{iter}}}\mathbf{D}^{l-1}\mathbf{H}\right)}_{\mathbf{S}}\mathbf{e}_{fs}^{n,n_{\text{iter}}},\end{aligned} \tag{92}$$

where $\mathbf{e}^{n+1,0}$ is written as $(\mathbf{x}_f^{n+1}-\mathbf{x}_f^{n})+(\mathbf{x}_f^{n}-\mathbf{x}_s^{n,n_{\text{iter}}})$. By recursion, $\mathbf{e}^{n+1,n_{\text{iter}}}$ is expressed in terms of the initial error $\mathbf{e}_{fs}^{0,0}$, $\mathbf{D}^{n_{\text{iter}}}$, and $\mathbf{S}$ as:

$$\mathbf{e}_{fs}^{n+1,n_{\text{iter}}}=\sum_{l=0}^{n}\mathbf{D}^{n_{\text{iter}}}\mathbf{S}^{l}\left(\mathbf{x}_f^{n+1-l}-\mathbf{x}_f^{n-l}\right)+\mathbf{S}^{n+1}\mathbf{e}_{fs}^{0,0}. \tag{93}$$

Stability requires that $\|\mathbf{S}\|\leqslant 1$ and $\|\mathbf{D}^{n_{\text{iter}}}\|\leqslant 1$ [45]. For convergence analysis, we assume no initial error, such that $\|\mathbf{e}_{fs}^{0,0}\|=\|\mathbf{x}_f^{0}-\mathbf{x}_s^{0,0}\|=0$. By the triangular inequality:

$$\begin{aligned}\left\|\mathbf{e}_{fs}^{n+1,n_{\text{iter}}}\right\| &\leqslant \left\|\mathbf{D}^{n_{\text{iter}}}\right\|\sum_{l=0}^{n}\left\|\mathbf{x}_f^{n+1-l}-\mathbf{x}_f^{n-l}\right\| \leqslant \left\|\mathbf{D}^{n_{\text{iter}}}\right\|\sum_{l=0}^{n}M_1\Delta t\\ &= \left\|\mathbf{D}^{n_{\text{iter}}}\right\|M_1 t_{n+1}\\ &\quad(\text{since } \mathbf{x}_f^{n+1}=\mathbf{x}_f^{n}+O(\Delta t)\quad\text{from the Taylor expansion}),\end{aligned} \tag{94}$$

where M_1 is a positive constant independent of time step size, and t_n is the simulation time up to the n^{th} time step. Thus, $\|\mathbf{e}_{fs}^{n+1,n_{\text{iter}}}\|=O(1)$ when $\|\mathbf{D}\|=O(1)$. As the time step size goes to zero:

$$\lim_{\Delta t\to 0}\|\mathbf{D}\|\neq 0,$$

which yields $\|\mathbf{D}\|=O(1)$ in Eq. (91), Non-convergence of the drained split for a fixed number of iterations was originally anticipated by Turska et al. [45]. They pointed out that $\|\mathbf{D}\|=O(1)$ implies non-convergence whereas $\|\mathbf{D}\|=O(\Delta t)$ shows convergence.

The fact that $\|\mathbf{D}\|=O(1)$ can also be derived from the error amplification factor as shown in the next section. Thus, the drained split with a fixed iteration number is not convergent. In particular, the drained split can show severe non-convergence problems as $\|\mathbf{D}\|$ approaches one, which is the stability limit of the drained split.

Remark 5. Turska et al. [45] and Turska and Schrefler [70] indicate that $\|\mathbf{D}\|\leqslant 1$ for convergence of sequential methods during iterations and $\|\mathbf{S}\|\leqslant 1$ for stability of sequential methods. Here, we define convergence as global convergence of a numerical solution, and stability as the condition for bounding the numerical errors. Hence, we require that $\|\mathbf{D}\|\leqslant 1$ and $\|\mathbf{S}\|\leqslant 1$ for stability, and $\lim_{\Delta t\to 0}\|\mathbf{D}\|=0$ for convergence.

8.2. Error estimation of the undrained split by matrix algebra

In the undrained split, matrix $\mathbf{A}$ in Eq. (89) is decomposed into:

$$\begin{bmatrix}\mathbf{K}+\mathbf{L}^t\mathbf{Q}^{-1}\mathbf{L} & \mathbf{0}\\ \mathbf{L} & \mathbf{F}\end{bmatrix}\begin{bmatrix}\mathbf{u}\\ \mathbf{p}\end{bmatrix}^{n+1,k+1} - \begin{bmatrix}\mathbf{L}^t\mathbf{Q}^{-1}\mathbf{L} & \mathbf{L}^t\\ \mathbf{0} & \mathbf{0}\end{bmatrix}\begin{bmatrix}\mathbf{u}\\ \mathbf{p}\end{bmatrix}^{n+1,k} - \begin{bmatrix}\mathbf{0} & \mathbf{0}\\ \mathbf{L} & \mathbf{Q}\end{bmatrix}\begin{bmatrix}\mathbf{u}\\ \mathbf{p}\end{bmatrix}^{n} = \begin{bmatrix}\mathbf{f}_{\mathbf{u}}\\ \mathbf{f}_{\mathbf{p}}\end{bmatrix}^{n+1}. \tag{95}$$

Let $\mathbf{K}_{ud}=\mathbf{K}+\mathbf{L}^t\mathbf{Q}^{-1}\mathbf{L}$. Then the errors can be expressed as:

$$\begin{aligned}\begin{bmatrix}\mathbf{e}_{fs,\mathbf{u}}\\ \mathbf{e}_{fs,\mathbf{p}}\end{bmatrix}^{n+1,k+1} &= \begin{bmatrix}\mathbf{K}_{ud} & \mathbf{0}\\ \mathbf{L} & \mathbf{F}\end{bmatrix}^{-1}\\ &\quad\times\left(\begin{bmatrix}\mathbf{L}^t\mathbf{Q}^{-1}\mathbf{L} & \mathbf{L}^t\\ \mathbf{0} & \mathbf{0}\end{bmatrix}\begin{bmatrix}\mathbf{e}_{fs,\mathbf{u}}\\ \mathbf{e}_{fs,\mathbf{p}}\end{bmatrix}^{n+1,k} + \begin{bmatrix}\mathbf{0} & \mathbf{0}\\ \mathbf{L} & \mathbf{Q}\end{bmatrix}\begin{bmatrix}\mathbf{e}_{fs,\mathbf{u}}\\ \mathbf{e}_{fs,\mathbf{p}}\end{bmatrix}^{n}\right)\\ &= \begin{bmatrix}\mathbf{K}_{ud}^{-1} & \mathbf{0}\\ -\mathbf{F}^{-1}\mathbf{L}\mathbf{K}_{ud}^{-1} & \mathbf{F}^{-1}\end{bmatrix}\\ &\quad\times\left(\begin{bmatrix}\mathbf{L}^t\mathbf{Q}^{-1}\mathbf{L} & \mathbf{L}^t\\ \mathbf{0} & \mathbf{0}\end{bmatrix}\begin{bmatrix}\mathbf{e}_{fs,\mathbf{u}}\\ \mathbf{e}_{fs,\mathbf{p}}\end{bmatrix}^{n+1,k} + \begin{bmatrix}\mathbf{0} & \mathbf{0}\\ \mathbf{L} & \mathbf{Q}\end{bmatrix}\begin{bmatrix}\mathbf{e}_{fs,\mathbf{u}}\\ \mathbf{e}_{fs,\mathbf{p}}\end{bmatrix}^{n}\right)\\ &= \underbrace{\begin{bmatrix}\mathbf{K}_{ud}^{-1}\mathbf{L}^t\mathbf{Q}^{-1}\mathbf{L} & \mathbf{K}_{ud}^{-1}\mathbf{L}^t\\ -\mathbf{F}^{-1}\mathbf{L}\mathbf{K}_{ud}^{-1}\mathbf{L}^t\mathbf{Q}^{-1}\mathbf{L} & -\mathbf{F}^{-1}\mathbf{L}\mathbf{K}_{ud}^{-1}\mathbf{L}^t\end{bmatrix}}_{\mathbf{D}_{ud}}\begin{bmatrix}\mathbf{e}_{fs,\mathbf{u}}\\ \mathbf{e}_{fs,\mathbf{p}}\end{bmatrix}^{n+1,k}\\ &\quad+\begin{bmatrix}\mathbf{0} & \mathbf{0}\\ \mathbf{F}^{-1}\mathbf{L} & \mathbf{F}^{-1}\mathbf{Q}\end{bmatrix}\begin{bmatrix}\mathbf{e}_{fs,\mathbf{u}}\\ \mathbf{e}_{fs,\mathbf{p}}\end{bmatrix}^{n}.\end{aligned} \tag{96}$$

From the first row of Eq. (96), we have:

$$\begin{aligned}\mathbf{e}_{fs,\mathbf{u}}^{n+1,k+1} &= \mathbf{K}_{ud}^{-1}\mathbf{L}^t\mathbf{Q}^{-1}\mathbf{L}\mathbf{e}_{fs,\mathbf{u}}^{n+1,k} + \mathbf{K}_{ud}^{-1}\mathbf{L}^t\mathbf{e}_{fs,\mathbf{p}}^{n+1,k} \\ &= \mathbf{K}_{ud}^{-1}\mathbf{L}^t\left(\mathbf{Q}^{-1}\mathbf{L}\mathbf{e}_{fs,\mathbf{u}}^{n+1,k} + \mathbf{e}_{fs,\mathbf{p}}^{n+1,k}\right). \end{aligned} \tag{97}$$

$\mathbf{F}^{-1}\mathbf{L}$ times the first row of Eq. (96) plus the second row of Eq. (96) yields:

$$\mathbf{F}^{-1}\mathbf{L}\mathbf{e}_{fs,\mathbf{u}}^{n+1,k+1} + \mathbf{e}_{fs,\mathbf{p}}^{n+1,k+1} = \mathbf{F}^{-1}\mathbf{L}\mathbf{e}_{fs,\mathbf{u}}^{n} + \mathbf{F}^{-1}\mathbf{Q}\mathbf{e}_{fs,\mathbf{p}}^{n}. \tag{98}$$

Note that $\mathbf{F} \to \mathbf{Q}$ as $\Delta t \to 0$ since $\lim_{\Delta t\to 0}\{\Delta t\mathbf{T}\} = \mathbf{0}$ in Eq. (89). Using Eqs. (97) and (98), the pressure error, $\mathbf{e}_{fs,\mathbf{p}}$, becomes:

$$\begin{aligned}\lim_{\Delta t\to 0}\mathbf{e}_{fs,\mathbf{p}}^{n+1,k+1} &= \lim_{\Delta t\to 0}\left(-\mathbf{F}^{-1}\mathbf{L}\mathbf{e}_{fs,\mathbf{u}}^{n+1,k+1} + \mathbf{F}^{-1}\mathbf{L}\mathbf{e}_{fs,\mathbf{u}}^{n} + \mathbf{F}^{-1}\mathbf{Q}\mathbf{e}_{fs,\mathbf{p}}^{n}\right) \\ &\quad \text{(from (98))} \\ &= -\mathbf{Q}^{-1}\mathbf{L}\underbrace{\mathbf{K}_{ud}^{-1}\mathbf{L}^t\left(\mathbf{Q}^{-1}\mathbf{L}\mathbf{e}_{fs,\mathbf{u}}^{n} + \mathbf{Q}^{-1}\mathbf{Q}\mathbf{e}_{fs,\mathbf{p}}^{n}\right)}_{\text{from (97)}} + \mathbf{Q}^{-1}\mathbf{L}\mathbf{e}_{fs,\mathbf{u}}^{n} \\ &\quad + \mathbf{Q}^{-1}\mathbf{Q}\mathbf{e}_{fs,\mathbf{p}}^{n} = \left(\mathbf{I} - \mathbf{Q}^{-1}\mathbf{L}\mathbf{K}_{ud}^{-1}\mathbf{L}^t\right)\left(\mathbf{Q}^{-1}\mathbf{L}\mathbf{e}_{fs,\mathbf{u}}^{n} + \mathbf{e}_{fs,\mathbf{p}}^{n}\right). \end{aligned} \tag{99}$$

As the time step size is refined to zero, Eq. (98) yields:

$$\lim_{\Delta t\to 0}\left(\mathbf{F}^{-1}\mathbf{L}\mathbf{e}_{fs,\mathbf{u}}^{n+1,k+1} + \mathbf{e}_{fs,\mathbf{p}}^{n+1,k+1}\right) = \mathbf{Q}^{-1}\mathbf{L}\mathbf{e}_{fs,\mathbf{u}}^{n} + \mathbf{e}_{fs,\mathbf{p}}^{n}. \tag{100}$$

From Eq. (100), the displacement error, $\mathbf{e}_{fs,\mathbf{u}}$, in Eq. (97), using $\lim_{\Delta t\to 0}\mathbf{F} = \mathbf{Q}$, becomes:

$$\begin{aligned}\lim_{\Delta t\to 0}\mathbf{e}_{fs,\mathbf{u}}^{n+1,k+1} &= \lim_{\Delta t\to 0}\mathbf{K}_{ud}^{-1}\mathbf{L}^t\left(\mathbf{Q}^{-1}\mathbf{L}\mathbf{e}_{fs,\mathbf{u}}^{n+1,k} + \mathbf{e}_{fs,\mathbf{p}}^{n+1,k}\right) \\ &= \mathbf{K}_{ud}^{-1}\mathbf{L}^t\left(\mathbf{Q}^{-1}\mathbf{L}\mathbf{e}_{fs,\mathbf{u}}^{n} + \mathbf{e}_{fs,\mathbf{p}}^{n}\right). \end{aligned} \tag{101}$$

Then, from Eqs. (99) and (101), the displacement and pressure errors become:

$$\begin{bmatrix}\mathbf{e}_{fs,\mathbf{u}} \\ \mathbf{e}_{fs,\mathbf{p}}\end{bmatrix}^{n+1,k+1} \overset{\Delta t\to 0}{\to} \underbrace{\begin{bmatrix}\mathbf{K}_{ud}^{-1}\mathbf{L}^t\mathbf{Q}^{-1}\mathbf{L} & \mathbf{K}_{ud}^{-1}\mathbf{L}^t \\ \left(\mathbf{I} - \mathbf{Q}^{-1}\mathbf{L}\mathbf{K}_{ud}^{-1}\mathbf{L}^t\right)\mathbf{Q}^{-1}\mathbf{L} & \mathbf{I} - \mathbf{Q}^{-1}\mathbf{L}\mathbf{K}_{ud}^{-1}\mathbf{L}^t\end{bmatrix}}_{\mathbf{E}_{ud}}\begin{bmatrix}\mathbf{e}_{fs,\mathbf{u}} \\ \mathbf{e}_{fs,\mathbf{p}}\end{bmatrix}^{n}. \tag{102}$$

By recursion and the assumption $\mathbf{e}_{fs}^{0,0} = 0$, $\mathbf{e}_{fs}^{n+1,n_{\text{iter}}}$, we can write:

$$\lim_{\Delta t\to 0}\left\|\mathbf{e}_{fs}^{n+1,n_{\text{iter}}}\right\| = \left\|\mathbf{E}_{ud}\mathbf{e}_{fs}^{n,n_{\text{iter}}}\right\| \leqslant \|\mathbf{E}_{ud}\|^n\|\mathbf{e}_{fs}^{0}\| = 0. \tag{103}$$

Eq. (103) implies that the undrained split yields convergence as the time step size is refined. Therefore, the undrained split is convergent with a fixed iteration number. We can also show convergence of the undrained split if $\|\mathbf{D}_{ud}\| = O(\Delta t)$, since $\|\mathbf{D}_{ud}\|$ corresponds to $\|\mathbf{D}\|$ in Eq. (94). In the next section we investigate the behavior of $\|\mathbf{D}_{ud}\|$ by spectral analysis. These results are easy to explain since, as the time step size goes to zero, the physical system approaches the undrained condition, and the undrained split converges to the fully coupled method regardless of how many iterations are taken.

Remark 6. Convergence of the undrained split is restricted to a (slightly) compressible system (i.e. compressible fluid or solid grains). When both the fluid and solid grains are incompressible, $\mathbf{Q} = 0$. As a result, $\mathbf{K}_{ud}^{-1}$ does not exist, and Eq. (103) is not valid for incompressible systems.

9. Spectral analysis

The matrix algebra method is a rather general approach to analyze whether a method is convergent, but it does not provide sharp information for the order of accuracy. In the previous sections, we saw that $\|\mathbf{D}\|$ and $\|\mathbf{D}_{ud}\|$ are the key parameters for convergence. In this section, we investigate $\|\mathbf{D}\|$ and $\|\mathbf{D}_{ud}\|$ further by performing an analysis of the error amplification of a 1D problem based on the finite volume and finite element methods adopted for flow and mechanics, respectively. The procedure is similar to the von Neumann method.

9.1. Error amplification of the drained split

The drained split treats the pressure term P^{n+1} in Eq. (33) explicitly as $P^{n+1,k}$, which is obtained from the previous iteration (k^{th}) step. The other variables in Eqs. (33) and (34) are treated implicitly as $U^{n+1,k+1}$ and $P^{n+1,k+1}$, which are unknown at the present $(k+1)^{th}$ step. Let $e_U^k = U^{n+1} - U^{n+1,k}$ and $e_P^k = P^{n+1} - P^{n+1,k}$, where U^{n+1} and P^{n+1} are the solutions from the fully coupled method, and $U^{n+1,k}$ and $P^{n+1,k}$ are those from the sequential methods at the kth iteration step. Let $e_P^{n,n_{\text{iter}}}$ and $e_U^{n,n_{\text{iter}}}$ be the difference between the solutions from the fully coupled and sequential methods at t_n for pressure and displacement, respectively. Then the error equations are given as:

$$-\frac{K_{dr}}{h}e_{U_{j-\frac{3}{2}}}^{k+1} + 2\frac{K_{dr}}{h}e_{U_{j-\frac{1}{2}}}^{k+1} - \frac{K_{dr}}{h}e_{U_{j+\frac{1}{2}}}^{k+1} - b\left(e_{P_{j-1}}^{k} - e_{P_j}^{k}\right) = 0, \tag{104}$$

$$\frac{h}{M}\frac{e_{P_j}^{k+1}}{\Delta t} + b\frac{h}{\Delta t}\left(-\frac{e_{U_{j-\frac{1}{2}}}^{k+1} - e_{U_{j+\frac{1}{2}}}^{k+1}}{h}\right) - \frac{k_p}{\mu}\frac{1}{h}\left(e_{P_{j+1}}^{k+1} - 2e_{P_j}^{k+1} + e_{P_{j-1}}^{k+1}\right) - \frac{h}{M}\frac{e_{P_j}^{n,n_{\text{iter}}}}{\Delta t} - b\frac{h}{\Delta t}\left(-\frac{e_{U_{j-\frac{1}{2}}}^{n,n_{\text{iter}}} - e_{U_{j+\frac{1}{2}}}^{n,n_{\text{iter}}}}{h}\right) = 0. \tag{105}$$

We set $e_P^{n,n_{\text{iter}}}$ and $e_U^{n,n_{\text{iter}}}$ to zero in order to investigate $\|\mathbf{D}\|$ in Eq. (91) only. This implies that we drop the second term in Eq. (91). Introducing errors of the form $e_{U_j}^k = \gamma_e^k e^{i(j)\theta}\widehat{e_U}$ and $e_{P_j}^k = \gamma_e^k e^{i(j)\theta}\widehat{e_P}$, where γ_e is the amplification factor of error, we obtain from Eqs. (104) and (105):

$$\underbrace{\begin{bmatrix}\frac{K_{dr}}{h}2\gamma_e(1-\cos\theta) & b2i\sin\frac{\theta}{2} \\ b\gamma_e 2i\sin\frac{\theta}{2} & \left[\frac{1}{M}h + \frac{k_p\Delta t}{\mu}\frac{1}{h}2(1-\cos\theta)\right]\gamma_e\end{bmatrix}}_{\mathbf{B}_{dr}}\begin{bmatrix}\widehat{e_U^k} \\ \widehat{e_P^k}\end{bmatrix} = \begin{bmatrix}0 \\ 0\end{bmatrix}. \tag{106}$$

Since the matrix $\mathbf{B}_{dr}$ is required to be singular (i.e., $\det\mathbf{B}_{dr} = 0$), this leads to:

$$\gamma_e = 0, \quad -\frac{b^2}{K_{dr}\left(\frac{1}{M} + \chi 2(1-\cos\theta)\right)}, \quad \chi = \frac{k_p\Delta t}{\mu h^2}. \tag{107}$$

The coefficient γ_e is equivalent to the eigenvalue of the error amplification matrix $\mathbf{G}$ defined by

$$\begin{bmatrix}e_{U_j}^{k+1} \\ e_{P_j}^{k+1}\end{bmatrix} = \mathbf{G}\begin{bmatrix}e_{U_j}^{k} \\ e_{P_j}^{k}\end{bmatrix}. \tag{108}$$

If the two γ_e's in Eq. (107) are distinct, then $\mathbf{G}$ can be decomposed as $\mathbf{G} = \mathbf{P}\Lambda\mathbf{P}^{-1}$ [71], where $\Lambda = \text{diag}\{\gamma_{e,1}, \gamma_{e,2}\}$ and $\mathbf{P}$ is an invertible matrix. When a fixed iteration number, $k = n_{\text{iter}}$, is used, the error estimate of the drained split is

$$\left\|\mathbf{e}_{fs}^{n+1,n_{\text{iter}}}\right\| \leqslant (\max|\gamma_e|)^{n_{\text{iter}}}\left\|\mathbf{e}_{fs}^{n+1,0}\right\|, \tag{109}$$

where $\mathbf{e}_{fs}^{n+1,0} = \mathbf{x}_f^{n+1} - \mathbf{x}_s^{n,n_{\text{iter}}}$. Thus, $(\max|\gamma_e|)$ is equivalent to $\|\mathbf{D}\|$.

Remark 7. From Eq. (94), $\mathbf{e}_{fs}^{n,n_{\text{iter}}}$ does not disappear even though Δt approaches zero, because $(\max|\gamma_e|)^{n_{\text{iter}}}$ does not approach zero (i.e., $O(1)$). Thus, the drained split with a fixed number of iterations is not convergent. Non-convergence of the drained split becomes

severe when $\max|\gamma_e|$ approaches one, which is also the same as the stability limit.

Remark 8. $\|\mathbf{D}\|$ is less than one if $\max|\gamma_e| \leqslant 1$ for all θ, which yields the stability condition of the drained split during iterations. In order to have $\max|\gamma_e| \leqslant 1$ for all θ in Eq. (107), the stability condition is $\tau = b^2 M/K_{dr} \leqslant 1$, where τ is the coupling strength. This stability condition coincides with that obtained by the von Neumann method.

9.2. Comparison with coupled flow and fully-dynamic geomechanics

The governing equations of coupled flow and fully-dynamic geomechanics are [30]:

$$\mathrm{Div}\,\boldsymbol{\sigma} + \rho_b \mathbf{g} = \rho_b \ddot{\mathbf{u}}, \tag{110}$$

$$\dot{m} + \mathrm{Div}\,\mathbf{w} = \rho_{f,0} f, \tag{111}$$

where $\ddot{(\cdot)}$ denotes the second order time derivative. Denote $\dot{\mathbf{u}}$ by $\mathbf{v}_k$, which is the rate of the solid skeleton displacement. Then, applying the fully coupled and drained split methods to Eqs. (110) and (111) and following the same procedure of the previous section, we obtain the following error equations:

$$e^{k+1}_{U_{j-\frac{1}{2}}} = \Delta t e^{k+1}_{V_{j-\frac{1}{2}}}, \tag{112}$$

$$e^{k+1}_{V_{j-\frac{1}{2}}} = \frac{\Delta t K_{dr}}{\rho_b h^2}\left(e^{k+1}_{U_{j-\frac{3}{2}}} - 2e^{k+1}_{U_{j-\frac{1}{2}}} + e^{k+1}_{U_{j+\frac{1}{2}}}\right) + \frac{\Delta t b}{\rho_b h}\left(e^{k}_{P_{j-1}} - e^{k}_{P_j}\right), \tag{113}$$

$$e^{k+1}_{P_j} = \frac{\Delta t M k_p}{\mu h^2}\left(e^{k+1}_{P_{j-1}} - 2e^{k+1}_{P_j} + e^{k+1}_{P_{j+1}}\right) + \frac{\Delta t M b}{h}\left(e^{k+1}_{V_{j-\frac{1}{2}}} - e^{k+1}_{V_{j+\frac{1}{2}}}\right), \tag{114}$$

where $V = \dot{U}$, $e^k_V = V^{n+1} - V^{n+1,k}$, and we assume the difference between the solutions from the fully coupled and sequential methods at t_n to be zero, as in the previous section. Introducing errors of the form $e^k_{U_j} = \gamma^k_e e^{i(j)\theta}\widehat{e_U}$, $e^k_{V_j} = \gamma^k_e e^{i(j)\theta}\widehat{e_V}$, and $e^k_{P_j} = \gamma^k_e e^{i(j)\theta}\widehat{e_P}$, we obtain:

$$\underbrace{\begin{bmatrix} \gamma_e & -\Delta t\gamma_e & 0 \\ \frac{\Delta t K_{dr}}{\rho_b h^2}2(1-\cos\theta)\gamma_e & \gamma_e & \frac{\Delta t b}{\rho_b h}2i\sin\frac{\theta}{2} \\ 0 & \frac{\Delta t M b}{h}2i\sin\frac{\theta}{2}\gamma_e & \gamma_e + \frac{\Delta t M k_p}{\mu h^2}2(1-\cos\theta)\gamma_e \end{bmatrix}}_{\mathbf{B}^*_{dr}} \times \begin{bmatrix} \widehat{e_U} \\ \widehat{e_V} \\ \widehat{e_P} \end{bmatrix} = \begin{bmatrix} 0 \\ 0 \\ 0 \end{bmatrix}. \tag{115}$$

From $\det(\mathbf{B}^*_{dr}) = 0$, the error amplification factors of the coupled flow and dynamics for the drained split are given by

$$\gamma_e = 0, \quad -\frac{\frac{\Delta t^2 M b^2}{\rho_b h^2}2(1-\cos\theta)}{\left(1 + \frac{\Delta t^2 K_{dr}}{\rho_b h^2}2(1-\cos\theta)\right)\left(1 + \frac{\Delta t M k_p}{\mu h^2}2(1-\cos\theta)\right)}. \tag{116}$$

Eq. (116) indicates that:

$$\lim_{\Delta t\to 0} \max|\gamma_e| = 0. \tag{117}$$

Following a similar procedure to that used for the drained split of quasi-static geomechanics (Eqs. (92)–(94)) and add $\mathbf{v}_k$ to the unknowns, one can show that the drained split for coupled flow and dynamics is convergent because $\lim_{\Delta t\to 0}\|\mathbf{e}^{n+1}_{fs}\| = 0$. As explained by Armero and Simo [30], when we use the staggered method (i.e., one iteration), convergence and first-order accuracy can be also directly estimated by Lie's formula [43,44]. Thus, the drained split of the coupled flow and dynamics is convergent, whereas the drained split of the coupled flow and quasi-static mechanics is not convergent, especially close to the stability limit.

Remark 9. A necessary condition for stability is $\max|\gamma_e| \leqslant 1$ for all θ in Eq. (116). To compare with the stability estimate of thermo-elasticity in Armero and Simo [30], consider the undrained limit corresponding to $k_p = 0$. Then the stability condition becomes:

$$\left\{2a_s\frac{\Delta t}{h}\right\}^2(\tau - 1) \leqslant 1, \tag{118}$$

where $a_s^2 = \frac{K_{dr}}{\rho_b}$, and a_s is the speed of sound [58]. Eq. (118) has a similar form to that of Armero and Simo [30]. The slight difference between the two is due to the different space and time discretization. In contrast to coupled flow and quasi-static mechanics, the stability of the drained split for the fully-dynamic case depends on the time step size. From Eq. (118), $\tau \leqslant 1$ can only provide stability as the mechanical problem approaches the elliptic limit (i.e., $\rho_b \to 0$, which yields $a_s \to \infty$), which is identical to the stability condition of coupled flow and statics. Furthermore, since one of the error amplification factors is negative, we may observe oscillations during iterations for the drained split in coupled flow and dynamics.

Remark 10. Even when both the fluid and solid grains are incompressible, $\lim_{\Delta t\to 0}\max|\gamma_e| = 0$. Hence, in contrast to coupled flow and statics, refining the time step size can recover stability and first-order accuracy for an incompressible problem.

9.3. Error amplification of the undrained split

The undrained split solves the mechanical problem while freezing fluid mass content for each grid block. Then the error equation for mechanics is written as:

$$-\frac{K_{ud}}{h}\left(e^{k+1}_{U_{j-\frac{3}{2}}} - 2e^{k+1}_{U_{j-\frac{1}{2}}} + e^{k+1}_{U_{j+\frac{1}{2}}}\right) + \frac{b^2 M}{h}\left(e^{k}_{U_{j-\frac{3}{2}}} - 2e^{k}_{U_{j-\frac{1}{2}}} + e^{k}_{U_{j+\frac{1}{2}}}\right) - b\left(e^{k}_{P_{j-1}} - e^{k}_{P_j}\right) = 0, \tag{119}$$

where $K_{ud} = K_{dr} + b^2 M$. The error equation for flow is the same as Eq. (105). Introducing errors of the form $e^k_{U_j} = \gamma^k_e e^{i(j)\theta}\widehat{e_U}$ and $e^k_{P_j} = \gamma^k_e e^{i(j)\theta}\widehat{e_P}$, Eqs. (119) and (105) yield:

$$\underbrace{\begin{bmatrix} \left(\frac{K_{dr}+b^2M}{h}\gamma_e - \frac{b^2 M}{h}\right)2(1-\cos\theta) & b2i\sin\frac{\theta}{2} \\ b\gamma_e 2i\sin\frac{\theta}{2} & \left[\frac{1}{M}h + \frac{k_p\Delta t}{\mu}\frac{1}{h}2(1-\cos\theta)\right]\gamma_e \end{bmatrix}}_{\mathbf{B}_{ud}} \times \begin{bmatrix} \widehat{e^k_U} \\ \widehat{e^k_P} \end{bmatrix} = \begin{bmatrix} 0 \\ 0 \end{bmatrix}. \tag{120}$$

From $\det\mathbf{B}_{ud} = 0$, the error amplification factors of the undrained split are obtained as:

$$\gamma_e = 0, \quad \frac{b^2\chi M 2(1-\cos\theta)}{(K_{dr} + b^2 M)\left(\frac{1}{M} + 2\chi(1-\cos\theta)\right)}. \tag{121}$$

From Eq. (121), when Δt is refined, $\max|\gamma_e|$ approaches zero. Since $\|\mathbf{D}_{ud}\| = \max|\gamma_e|$, $\mathbf{e}^n_{fs}$ goes to zero when the time step size is refined even if a fixed number of iterations is used. Hence, the undrained split with a fixed number of iterations exhibits first-order convergence for a compressible system.

Remark 11. We obtain first-order accuracy for the undrained split only for a compressible system. From Eq. (121), if the fluid and solid grains become incompressible, we have $M \to \infty$ and $\max|\gamma_e| \to 1$ regardless of time step size. Thus, we expect severe reductions of accuracy if the system is nearly incompressible ($M \to \infty$), and loss of convergence altogether for an incompressible system.

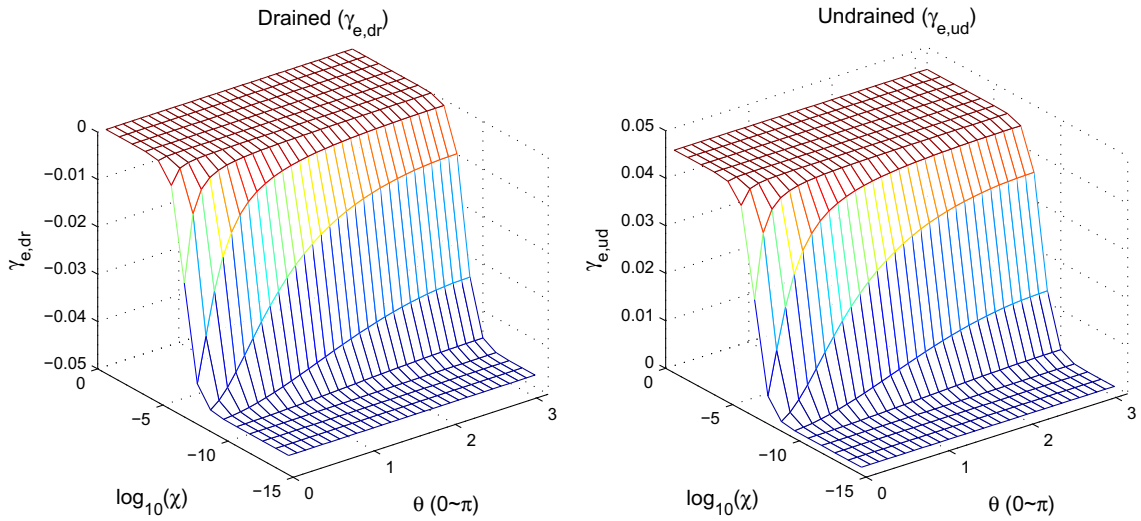

Fig. 3. The distribution of the error amplification factors of the drained (left) and undrained (right) splits with respect to pressure diffusivity χ and frequency. The coupling strength τ is 0.05.

Remark 12. The undrained split is always stable during iterations, since $\max|\gamma_e| \leqslant 1$ and γ_e's are distinct. Global unconditional stability is rigorously shown in the previous section on stability analysis.

10. Convergence rate of fully-iterated schemes

The solutions to the model equations of coupled flow and geomechanics using sequential methods converge to those of the fully coupled method when full iterations are performed if the schemes are stable and convergent during the iterative process. In this section, we address the question of which sequential method is more efficient in terms of the rate of convergence when full iterations are performed. The error amplification factors, shown in Eqs. (107) and (121), are appropriate tools for estimating the rate of convergence: smaller magnitudes indicate faster rates of convergence [49].

The left and right plots of Fig. 3 show the error amplification factors from Eq. (107) (drained split) and (121) (undrained split), for a coupling strength $\tau = 0.05$. The absolute value of the error amplification factor of the drained split, $|\gamma_{e,dr}|$, decreases with respect to χ in Eq. (107), where χ is pressure diffusivity. Hence, high (pressure) diffusive conditions (e.g., high permeability and large time step size) are favorable to the drained split in terms of the rate of convergence. However, $|\gamma_{e,ud}|$ of the undrained split increases with respect to χ, which implies that the undrained split exhibits better rates of convergence under less (pressure) diffusive conditions (e.g., low permeability and small time step size). Fig. 4 shows the difference between the magnitude of the two amplification factors, $|\gamma_{e,ud}| - |\gamma_{e,dr}|$. When the difference is negative, the undrained split shows a better rate of convergence compared with the drained split. When the difference is positive, the drained split shows better rates of convergence. From Fig. 4, it is apparent that the drained split can be faster than the undrained split for high χ, but the undrained split can be faster than the drained split for low χ.

11. Representative numerical examples

11.1. Stability behavior of the staggered approach

In this section, we confirm the results of the theoretical analysis by means of simple numerical examples. In Kim et al., [59] we show numerical simulations for linear poroelasticity – using staggered, non-iterative schemes – and nonlinear poroelastoplasticity – using various sequential schemes and full iteration to achieve convergence at each time step. In that work, a backward Euler time discretization was employed. Here we report simulations using the midpoint rule ($\alpha = 0.5$ for both mechanics and flow) and a mixed time discretization ($\alpha_{\text{mech}} = 1$ and $\alpha_{\text{flow}} = 0.5$). For the nonlinear problem, we concentrate exclusively on the non-iterative drained and undrained splits.

We report the results of three test cases:

Case 1.1 Fluid injection and withdrawal in a 1D elastic medium.
Case 1.2 Same as Case 1.1, but in a elastoplastic medium with isotropic hardening.
Case 1.3 Fluid withdrawal in a 2D elastoplastic medium, which induces compaction.

We only show the evolution of fluid pressure field because the displacement has the same stability characteristics as the pressure.

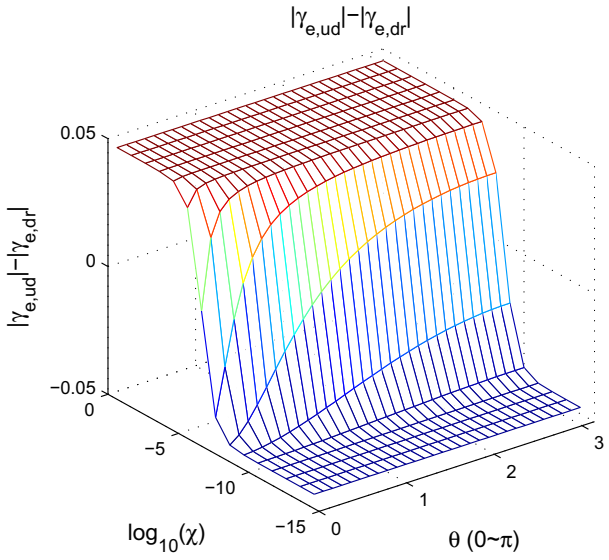

Fig. 4. The difference of the error amplification factors between the drained and undrained splits.

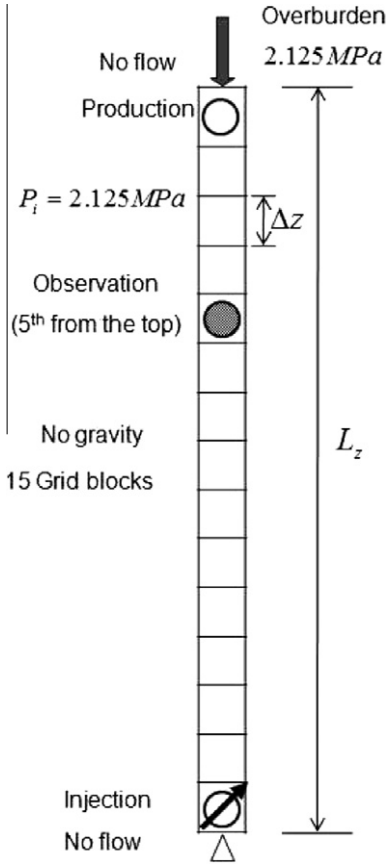

Fig. 5. Case 1.1: schematic of the problem of injection and production in a 1D medium.

11.1.1. Injection and withdrawal from 1D elastic medium

The first simulation example is a one-dimensional problem in which the deformation is driven by fluid injection and withdrawal. The schematic of the problem is shown in Fig. 5. A porous medium of thickness $L = 150$ m is subject to a constant overburden stress $\bar{\sigma} = 2.125$ MPa. The medium is assumed to be elastic, with a drained uniaxial modulus (constrained modulus) $K_{dr} = 1$ GPa. The permeability is $k = 50\ \text{md} \approx 5 \times 10^{-14}\ \text{m}^2$, and the porosity is $\phi_0 = 0.3$. Other parameters of the rock–fluid system are the Biot coefficient $b = 1$, the bulk density $\rho_b = 2400\ \text{kg m}^{-3}$, the fluid density $\rho_{f,0} = 1000\ \text{kg m}^{-3}$, and the fluid dynamic viscosity $\mu = 1\ \text{cP} = 10^{-3}$ Pa s. The fluid bulk modulus K_f – or, alternatively, the Biot modulus M – is left unspecified to test the performance of the drained and undrained splits for different values of the coupling strength τ (see Eq. (39)). We neglect gravity effects, and the initial pressure P_i is assumed to be uniform and equal to the overburden stress, so that the initial effective stress $\sigma'_0 = 0$ everywhere. The system is driven by injection and withdrawal of fluid from two wells, located at the bottom and top elements, respectively. We fix the injection and production mass fluxes, and take them as constant, $M_{\text{inj}} = M_{\text{prod}} = 100\ \text{kg m}^{-2}\ \text{day}^{-1}$ (in terms of volumetric flux, this corresponds to $Q \approx 1.16 \times 10^{-6}\ \text{ms}^{-1}$. We discretize the problem with 15 elements of equal size $\Delta z = 10$ m. We present results of the simulation in terms of the pressure evolution at an observation point, located at the center of the fifth element from the top of the domain.

Due to symmetry and linearity, the solution to the problem does not display overall subsidence of the porous medium. This does not mean that mechanical effects are unimportant: there is dilation around the injection well and compaction around the production well. Since the observation point is closer to the withdrawal well, the pressure at that point decreases with time.

In Fig. 6 we show the evolution of the pressure at this observation point. We plot the nondimensional pressure, $P_D \equiv P/P_i$, as a function of dimensionless time, $t_D \equiv t/t_c$, where the characteristic time is defined as $t_c = L/Q$ (therefore, t_D is simply the number of pore volumes injected). Results are for low coupling strength ($\tau = 0.083$), and two different time discretizations: backward Euler ($\alpha = 1$, left), and the midpoint rule ($\alpha = 0.5$, right). In agreement with the von Neumann stability analysis, the undrained split is stable for both values of α, given that $\tau < 1$. In contrast, the drained split is unstable if the midpoint rule is used, even for this very low value of the coupling strength – also in agreement with our analysis.

We now study the stability properties of the sequential schemes when a mixed time discretization is employed: a generalized midpoint rule with $\alpha = 1$ for the mechanics step and $\alpha = 0.5$ for the flow step. The von Neumann stability analysis suggests that this time discretization will be unconditionally stable if the

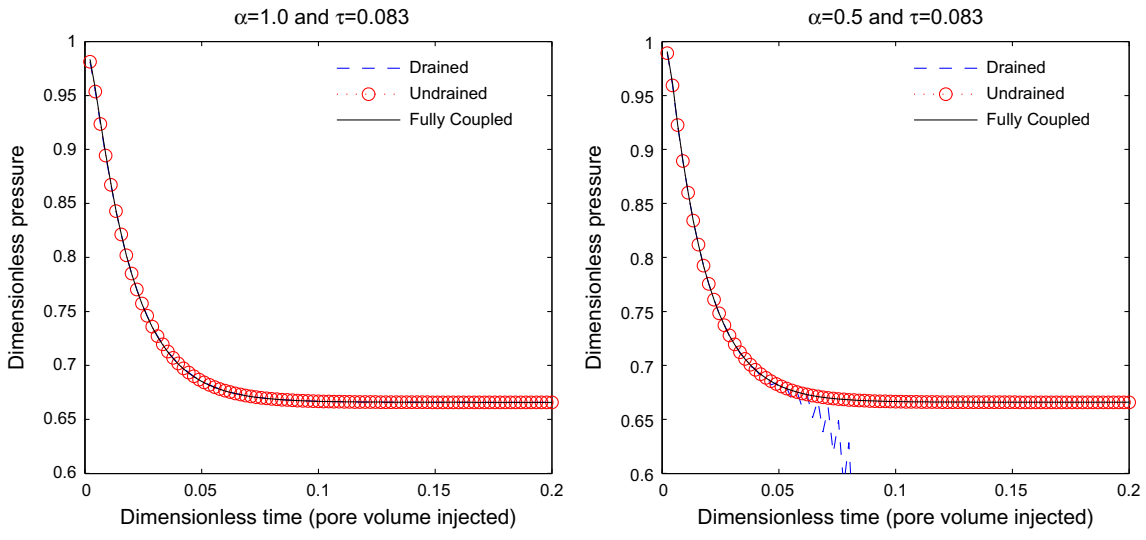

Fig. 6. Case 1.1: 1D poroelastic problem. Evolution of pressure at the observation point as a function of time. Results are for low coupling strength ($\tau = 0.083$), and two different time discretizations. Left: backward Euler ($\alpha = 1$); Right: midpoint rule ($\alpha = 0.5$). The undrained split is stable for both values of α. The drained split is unstable if the midpoint rule is used, even for this very low value of the coupling strength.

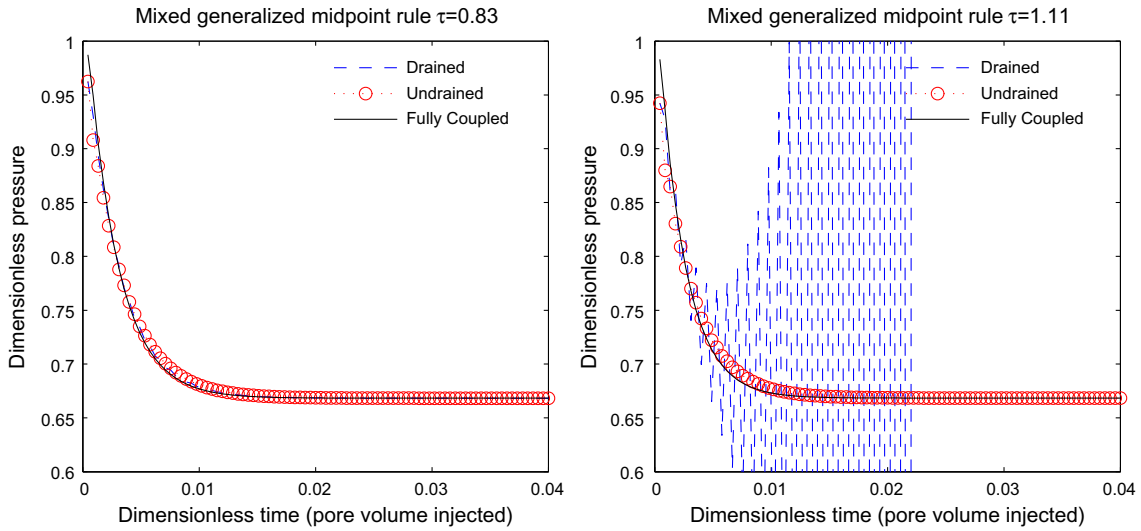

Fig. 7. Case 1.1: 1D poroelastic problem. Evolution of pressure at the observation point as a function of time. Results are for a mixed time discretization that uses a generalized midpoint rule with $\alpha = 1$ for the mechanics step and $\alpha = 0.5$ for the flow step. Left: coupling strength slightly less than one ($\tau = 0.83$); Right: coupling strength slightly greater than one ($\tau = 1.11$). The undrained split is stable for any value of τ. The drained split is unstable for $\tau > 1$.

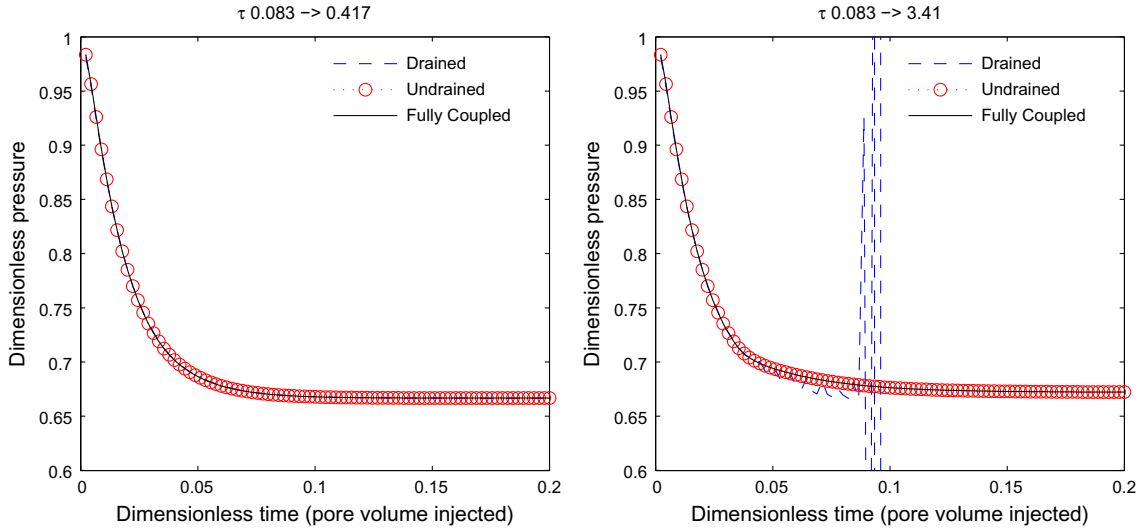

Fig. 8. Case 1.2: 1D poroelastoplastic problem. Evolution of pressure at the observation point as a function of time. Results are for a backward Euler time discretization ($\alpha = 1$). Left: coupling strength after plasticity less than one ($\tau = 0.417$); Right: coupling strength after plasticity greater than one ($\tau = 3.41$). The undrained split is stable for any value of τ, while the drained split becomes unstable after the material yields if $\tau > 1$. Stability of the drained split cannot be recovered by reducing the time step.

undrained split is used, but only conditionally stable ($\tau < 1$) if the drained split is employed. These results are confirmed by our numerical simulations (Fig. 7), which show that the undrained split is stable for any value of τ, and that the drained split is unstable for $\tau > 1$. The values we used for the coupling strength are only slightly less and slightly greater than one ($\tau = 0.83$ and $\tau = 1.11$, respectively), indicating that the criteria from the von Neumann stability analysis are sharp.

11.1.2. Injection and withdrawal from 1D elastoplastic medium

This test case is identical to the previous one, except that the medium is allowed to reach the plastic regime. We adopt an associated plasticity formulation with isotropic hardening [66,5]. The yield function f_Y is given by

$$f_Y = |\sigma'| - (\sigma'_Y + H\xi) = 0, \quad \text{with } \dot{\xi} = |\dot{\varepsilon}_p|, \tag{122}$$

where $H > 0$ is the hardening modulus. For the simulations, we take the values $\sigma'_Y = 1.5$ MPa, and $H = 250$ MPa and $H = 25$ MPa (corresponding to $\tau = 0.417$ and $\tau = 3.41$, respectively). The fundamental aspect of plasticity is that it softens the material and increases the coupling strength between flow and mechanics [26]. As a result, the coupling strength may increase in the course of a simulation from a value below 1 during the elastic response to a value above 1 when the material yields.

In Fig. 8 we show simulation results using backward Euler for two different cases: one in which the coupling strength remains below 1 when the material yields (left figure), and one in which it goes above 1 (right figure). In both cases, the medium enters the plastic regime at $t_D \approx 0.05$. It is apparent that the undrained split is stable – and follows the fully coupled solution almost exactly – independently of the value of τ. The drained split, in contrast, becomes unstable shortly after the material yields for the case in which the coupling strength jumps to a value above 1 (Fig. 8, right). The instability cannot be avoided by reducing the time step. These results are in full agreement with our nonlinear stability analysis.

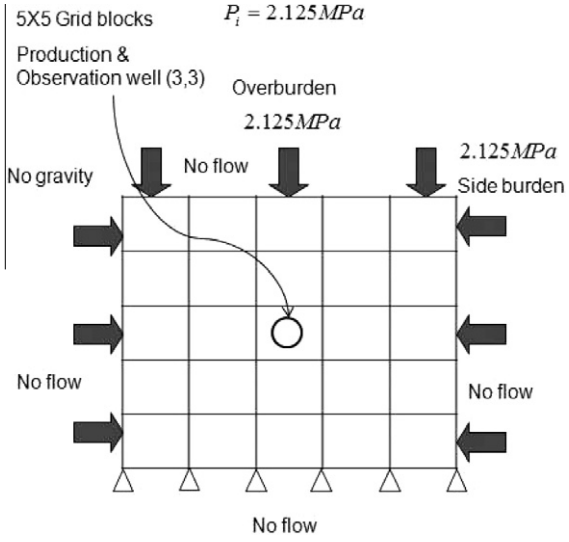

Fig. 9. Case 1.3: schematic of the problem of fluid production in a 2D medium.

11.1.3. Withdrawal from 2D elastoplastic medium

We model fluid withdrawal from the center of a 2D medium. The permeability is $k = 50$ md $\approx 5 \times 10^{-14}$ m^2, and the porosity is $\phi_0 = 0.3$. The Young modulus in the elastic regime is $E = 350$ MPa and the drained Poisson ratio is $\nu = 0.3$. Other parameters of the rock–fluid system are the Biot coefficient $b = 1$, the bulk density $\rho_b = 2400$ kg m^{-3}, the fluid density $\rho_{f,0} = 1000$ kg m^{-3}, and the fluid dynamic viscosity $\mu = 1$ cP $= 10^{-3}$ Pa s. The medium is elastoplastic, and modeled with a modified Cam-clay formulation [72]. The yield function is given by

$$f_Y = \frac{q'^2}{M_{\text{mcc}}^2} + \sigma'_v(\sigma'_v - p_{\text{co}}) = 0, \tag{123}$$

where q' is the deviatoric effective stress, σ'_v is the volumetric effective stress, M_{mcc} is the slope of the critical state line, and p_{co} is the preconsolidation pressure. In our simulations, we use the following parameter values: critical state slope $M_{\text{mcc}} = 1.4$, initial preconsolidation pressure $p_{\text{co}} = -1$ MPa, virgin compression index $\lambda = 0.37$, and swell index $\kappa = 0.054$. For details on the mathematical formulation and the implementation of the return-mapping algorithm for this poroelastoplastic model, see Borja and Lee [72].

The overburden $\bar{\sigma}_v$ and side burden stress $\bar{\sigma}_h$ are assumed to be equal, with a value of 2.125 MPa. The initial pressure is assumed to have the same value, $p_0 = 2.125$ MPa, so the initial effective stress is zero everywhere. The dimensions of the domain are 50×50 m, discretized with a simple 5×5 regular grid of rectangular elements (Fig. 9).

The numerical simulations of this third test case extend our previous findings to multidimensional problems. In Fig. 10 we show the evolution of dimensionless pressure at the center of the domain as a function of dimensionless time (left figure). We plot the solutions for the fully-coupled method with the Newton-Raphson method per time step, along with the solutions for the staggered method with the drained and undrained splits. The undrained split is stable throughout, and follows closely the fully-coupled solution. The drained split becomes unstable at $t_d \approx 0.018$. The reason for this behavior is explored on the right figure, which shows the evolution of the coupling strength τ as a function of time. Initially, in the elastic regime, the coupling strength is less than 1. The plastic regime is reached at time $t_d \approx 0.018$, and the coupling strength rises sharply to a value significantly larger than 1, causing the instability of the drained method.

11.2. Convergence behavior for a fixed number of iterations

We introduce two test cases to study the convergence behavior of the fully coupled, drained, and undrained methods. Cases 2.1 and 2.2 are one and two dimensional consolidation problems.

Case 2.1 One-dimensional consolidation problem in a linear poroelastic medium, the Terzaghi problem (the left picture in Fig. 11).

Case 2.2 Two-dimensional consolidation problem in a linear poroelastic medium (the right picture in Fig. 11).

The true (reference) solutions are computed using the fully coupled method with a very small time step size to minimize the temporal error. The analytic solution is available for Case 2.1. The reference solution matches the analytic solution within tight error tolerances.

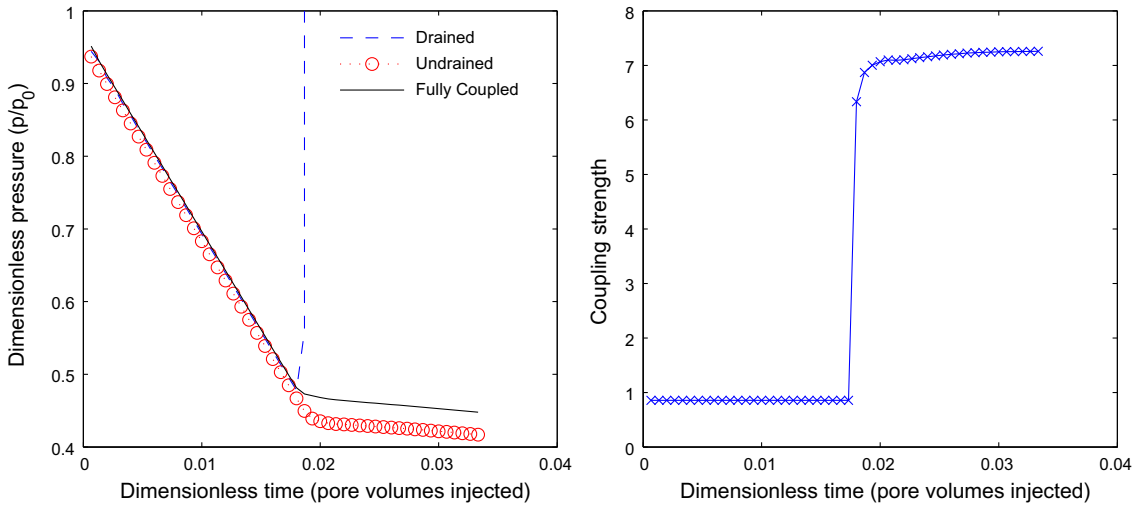

Fig. 10. Case 1.3: 2D poroelastoplastic problem. Results are for a backward Euler time discretization ($\alpha = 1$). Left: evolution of pressure at the observation point (center element) as a function of time. Shown are the solutions for the fully-coupled method with full iteration per time step, along with the solutions for the staggered method with the drained and undrained splits. The drained split becomes unstable at $t_d \approx 0.018$. Right: evolution of the coupling strength τ as a function of time. Initially, in the elastic regime, the coupling strength is less than 1. The plastic regime is reached at time $t_d \approx 0.018$, and the coupling strength rises sharply to a value significantly larger than 1.

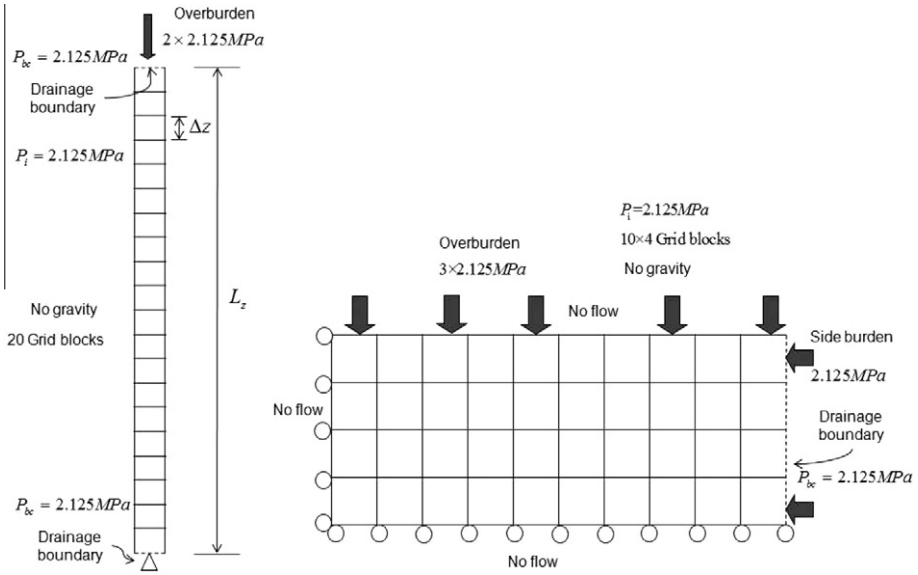

Fig. 11. Case 2.1: the Terzaghi problem in one dimension (left). Case 2.2: the consolidation problem in two dimensions (right).

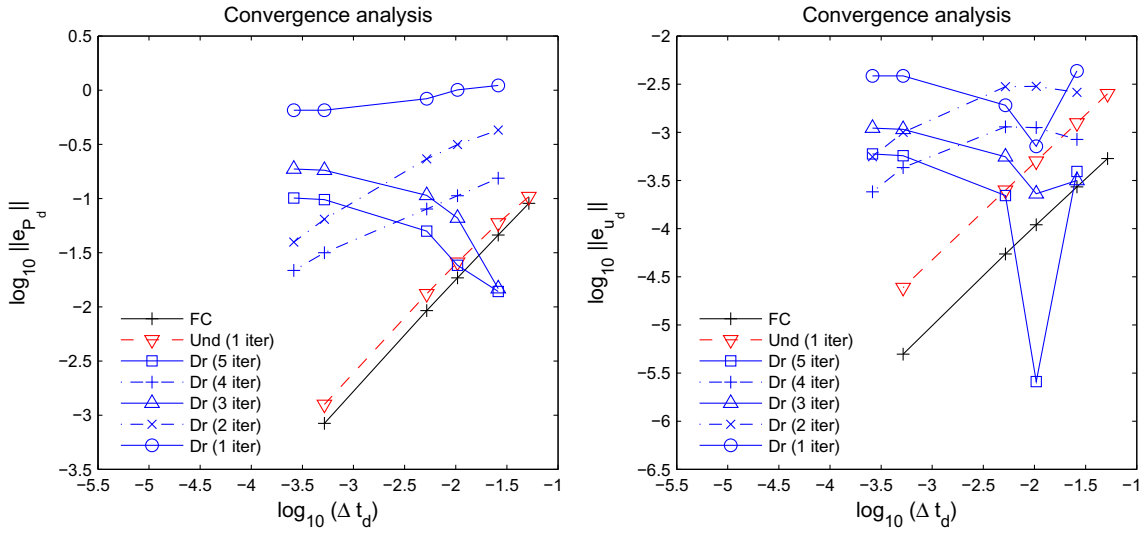

Fig. 12. Convergence analysis of Case 2.1 on pressure (left) and displacement (right). The coupling strength $\tau = b^2M/K_{dr}$, is 0.95. *FC*, *Dr*, and *Und* indicate the fully coupled, drained split, and undrained split methods, respectively. $\Delta t_d = 4c_v\,\Delta t/(L_z)^2$, where c_v is the consolidation coefficient defined as $c_v = \frac{k_p}{(1/K_{dr}+\phi c_f)\mu}$.

11.2.1. Case 2.1 – The Terzaghi problem

We have drainage boundaries for flow at the top and bottom, where the boundary fluid pressure is P_{bc} = 2.125 MPa. The overburden is $\bar{\sigma} = 4.250$ MPa at the top, and a no-displacement boundary condition is applied to the bottom. The initial fluid pressure is P_i = 2.125 MPa. The domain is discretized with 20 grid blocks. The length of the domain is L_z = 40 m with grid spacing Δz = 2 m. The bulk density of the porous medium is ρ_b = 2400 kg m^{-1}. The fluid density and viscosity are $\rho_{f,0}$ = 1000 kg m^{-1} and μ = 1.0 cp, respectively. The medium permeability is k_p = 50 md, the porosity is ϕ_0 = 0.3, the constrained modulus is K_{dr} = 100 MPa, and the Biot coefficient is b = 1.0. No production and injection of fluid is applied, and gravity is neglected. The Biot modulus is M = 95 MPa, where $c_f = 3.5 \times 10^{-8}$ Pa^{-1} and the coupling strength is τ = 0.95.

For Case 2.1, Fig. 12 illustrates the errors of the numerical solutions from the drained, undrained, and fully coupled methods with respect to time step size when a fixed number of iterations is performed. The errors of dimensionless pressure and displacement are measured by the L^2 norm. The undrained and fully coupled methods are convergent when a staggered method (i.e. one iteration) is used. As the time step size is refined, the errors decrease as $O(\Delta t)$. This confirms that the undrained and fully coupled methods have $O(\Delta t)$ accuracy in time. The drained split, however, does not converge. In particular, one iteration of the drained split yields zeroth-order accuracy, which supports the a priori error estimate. Figs. 13 and 14 show the spatial distributions of pressure and displacement by the drained and undrained splits, respectively. As the time step size is refined, the drained split with one iteration does not converge to the true solution, but to a different solution, even though the distributions of pressure and displacement look plausible. On the other hand, the undrained split with one iteration converges to the true solution. When an even number of iterations is used, the drained split exhibits better convergence in time than with an odd number of iterations. This is likely due to a phenomenon of

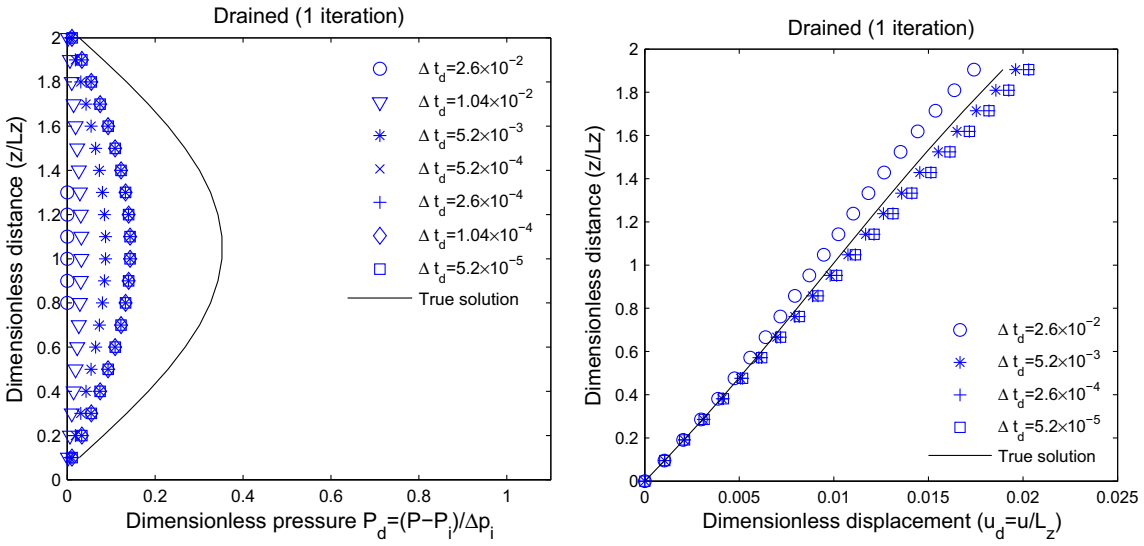

Fig. 13. Non-convergence of the drained split with one iteration for Case 2.1: pressure (left) and displacement (right).

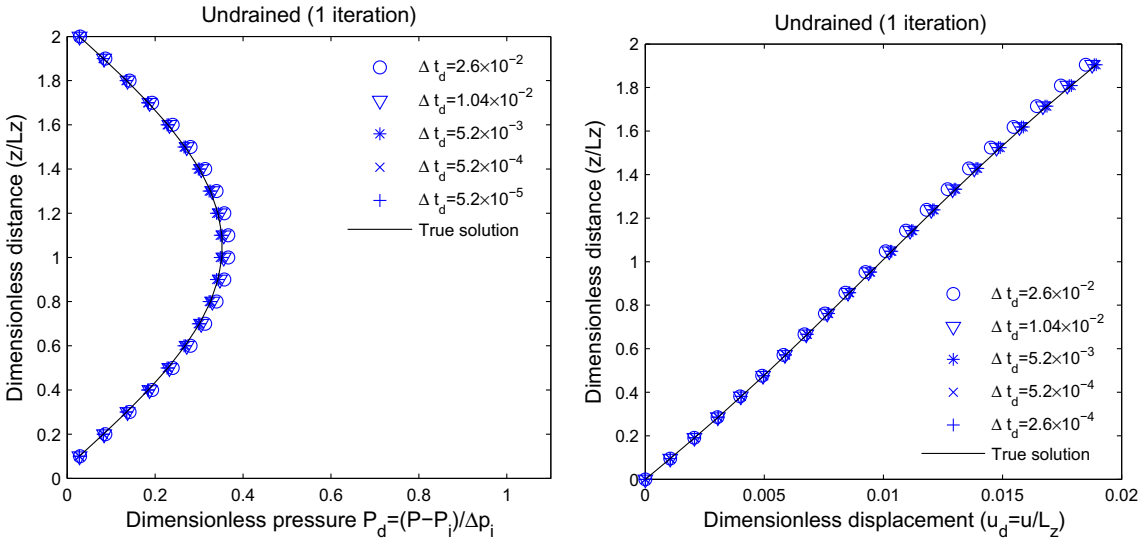

Fig. 14. Convergence of pressure for the undrained split with one iteration for Case 2.1: pressure (left) and displacement (right).

error cancellation that we have not investigated in detail. To illustrate this effect, Fig. 15 shows a comparison of the solutions obtained taking one and two iterations per time step. The time step size is doubled in the simulation with two iterations per time step, so that both simulations have the same computational cost.

11.2.2. Non-convergence of the undrained split for incompressible systems

From Eq. (121), we expect that the undrained split will exhibit convergence problems for an incompressible, or nearly incompressible, system. In Fig. 16, we observe zeroth-order accuracy for pressure and displacement for the nearly incompressible fluid, $c_f = 3.5 \times 10^{-13}\,\mathrm{Pa}^{-1}$. Fig. 16 shows clearly that undrained-split solutions do not converge to the true solutions. Non-convergence of the undrained split becomes severe when the fluid is incompressible, $c_f \cong 0$. Fig. 17 shows zeroth-order accuracy for pressure and displacement as well. The right panel of Fig. 17 shows that the undrained split predicts there is no pressure change. This is because there is no change of volumetric strain ε_v after solving the mechanical problem as a result of the undrained bulk modulus being infinite due to the incompressible fluid. Thus, the undrained split cannot solve the coupled problem in the incompressible limit because it fails to establish proper communication between the flow and mechanical problems.

11.2.3. Case 2.2 – Two dimensional consolidation problem

Case 2.2 is an example of two dimensional consolidation under plane-strain conditions, where the coupling strength approaches one ($\tau \lesssim 1$ where $c_f = 2.30 \times 10^{-9}\,\mathrm{Pa}^{-1}$). The dimension of the domain is 20×0.02 m and it is discretized with 10×4 grid blocks. The domain is assumed to be homogeneous. We impose an overburden stress $\bar{\sigma} = 6.375$ MPa at the top, no horizontal displacement on the left boundary, a side burden $\bar{\sigma}_h = 2.125$ MPa on the right boundary, and no vertical displacement boundary at the bottom boundary. The initial fluid pressure is $P_i = 2.125$ MPa. The bulk density of the porous medium is $\rho_b = 2400\,\mathrm{kg\,m}^{-1}$. The fluid

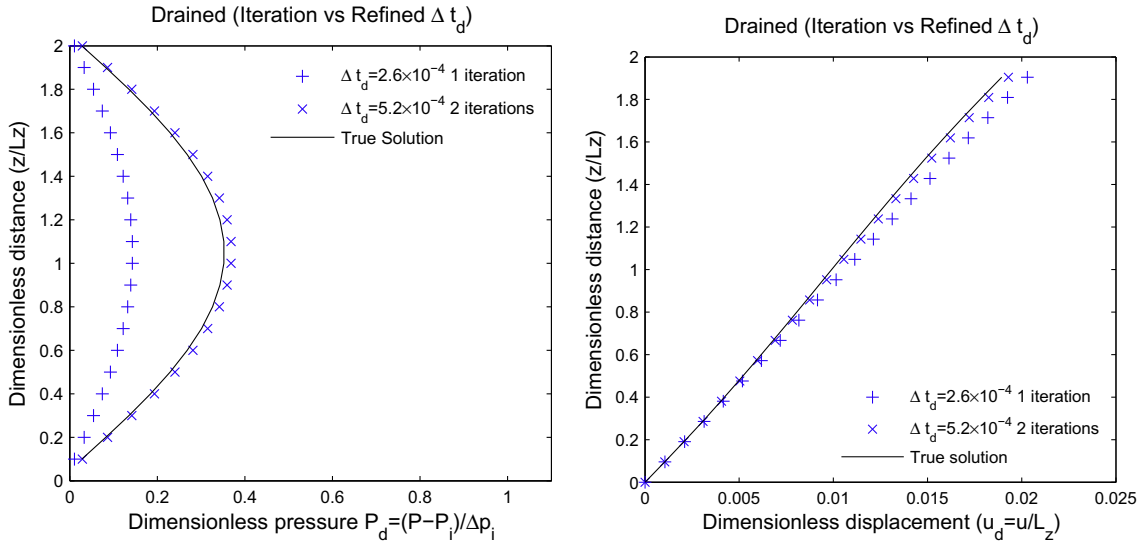

Fig. 15. Comparison between more iterations and refined time step size in the drained split for Case 2.1: pressure (left) and displacement (right).

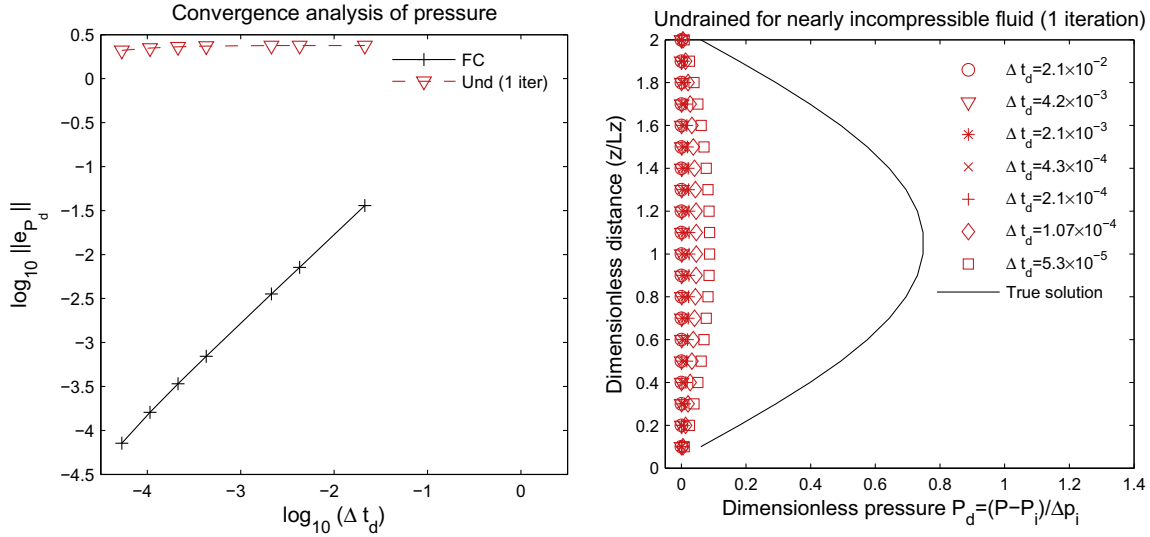

Fig. 16. Left: Convergence analysis of pressure for a nearly incompressible fluid, where $\tau = 9.5 \times 10^4$ and $c_f = 3.5 \times 10^{-13}$ Pa^{-1}. Right: Spatial distributions of pressure. The staggered method is used. The undrained split is not convergent, showing almost zeroth-order accuracy. The fully coupled method shows first-order accuracy.

density and viscosity are $\rho_{f0} = 1000$ kg m^{-1} and $\mu = 1.0$ cp, respectively. The medium permeability is $k_p = 5$ md, and the porosity is $\phi_0 = 0.3$. The Young modulus is $E = 2.9$ GPa, and Poisson's ratio is $\nu = 0.0$. The Biot coefficient is $b = 1.0$. We have a drainage boundary for flow on the right side where the boundary fluid pressure is $P_{bc} = 2.125$ MPa. No-flow boundary conditions are applied at the left side, top, and bottom, and the effect of gravity is neglected.

Since the layers are very thin, the fluid flows mainly along the horizontal direction. Fig. 18 shows the convergence behaviors of the drained and undrained splits for Case 2.2 when one single iteration is performed. The drained split shows zeroth-order accuracy in time, and the undrained split shows first-order accuracy. Non-convergence of the drained split can be clearly identified in the right panel of Fig. 18, which shows the distributions of pressure along the top layer. The solutions by the drained split with one iteration do not converge to the true solutions, even though the distributions look plausible. Thus, refining the time step size cannot improve the accuracy of the solutions by the drained split with one iteration. In contrast, increasing the number of iterations for a fixed time step size does improve the accuracy. The left of Fig. 19 compares a large time step size with more iterations ($\Delta t_d = 2.06 \times 10^{-3}$, 10 iterations) with a small time step size and one iteration ($\Delta t_d = 2.06 \times 10^{-4}$, one iteration). The two simulations have the same computational cost. $\Delta t_d = 2.06 \times 10^{-3}$ with 10 iterations provides higher accuracy matching the true solutions than $\Delta t_d = 2.06 \times 10^{-4}$ with one iteration. The right panel of Fig. 19 shows that the undrained-split solutions with one iteration converge to the true solutions.

11.3. Rate of convergence of fully-iterated schemes

We employ Cases 2.1 and 2.2 to study the rate of convergence of fully-iterated sequential schemes. For Case 2.1, Fig. 20 shows the variation of the maximum absolute values of the residuals with respect to the number of iteration under low (the left figure) and high (the right figure) pressure–diffusion conditions. The cou-

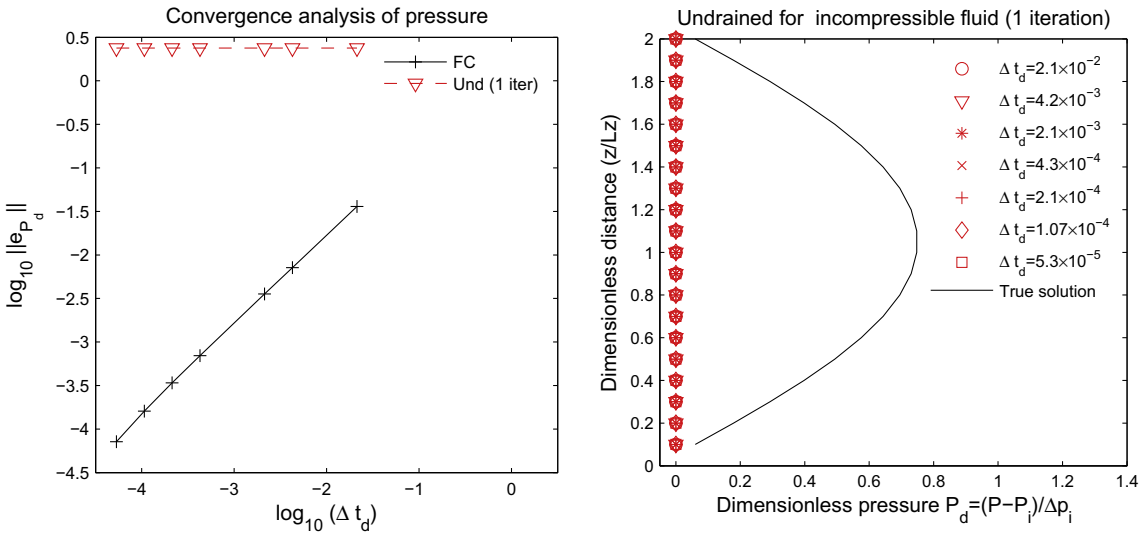

Fig. 17. Left: Convergence analysis of pressure (left) and displacement (right) for an incompressible fluid, where $\tau = 9.5 \times 10^{11} \cong \infty$ and $c_f = 3.5 \times 10^{-20}\,\mathrm{Pa}^{-1} \cong 0$. Right: Spatial distributions of pressure. The undrained split is not convergent, showing zeroth-order accuracy. But, the fully coupled method shows first-order accuracy.

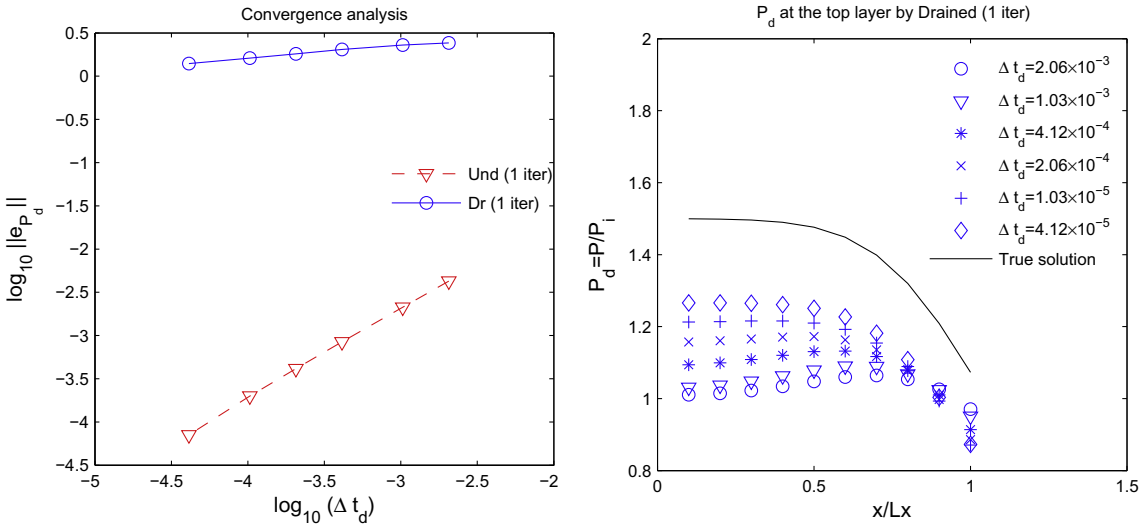

Fig. 18. Left: Convergence analysis of Case 2.2 on pressure. Right: spatial distributions of pressure in the drained split with one iteration. $P_d = P/P_i$ and $\Delta t_d = 4\Delta t c_v / L_x^2$, where c_v is the consolidation coefficient along the horizontal direction.

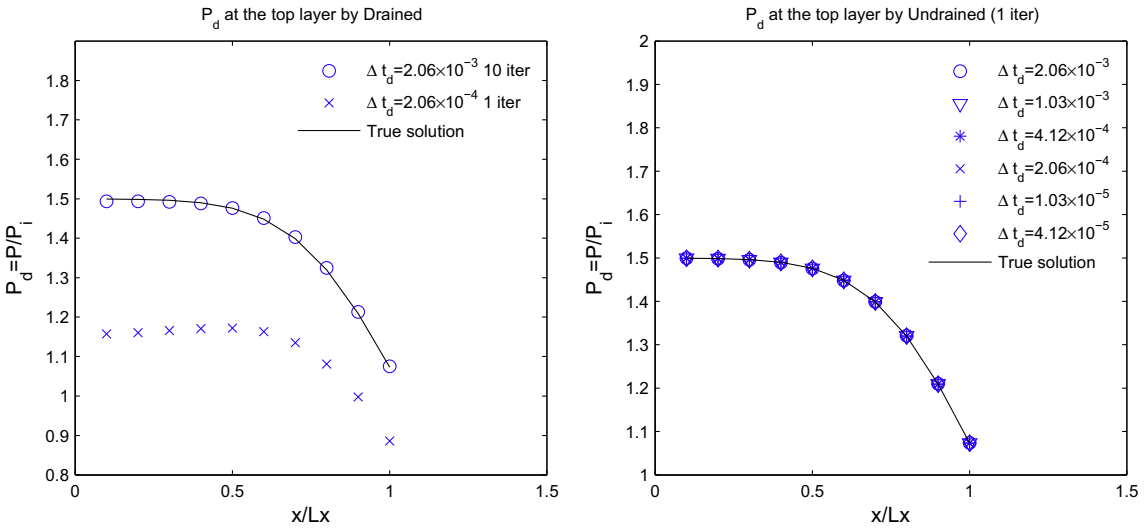

Fig. 19. Left: Comparison of pressure between more iterations and refined time step size in the drained split for Case 2.2. Right: Spatial distributions of pressure in the undrained split with one iteration.

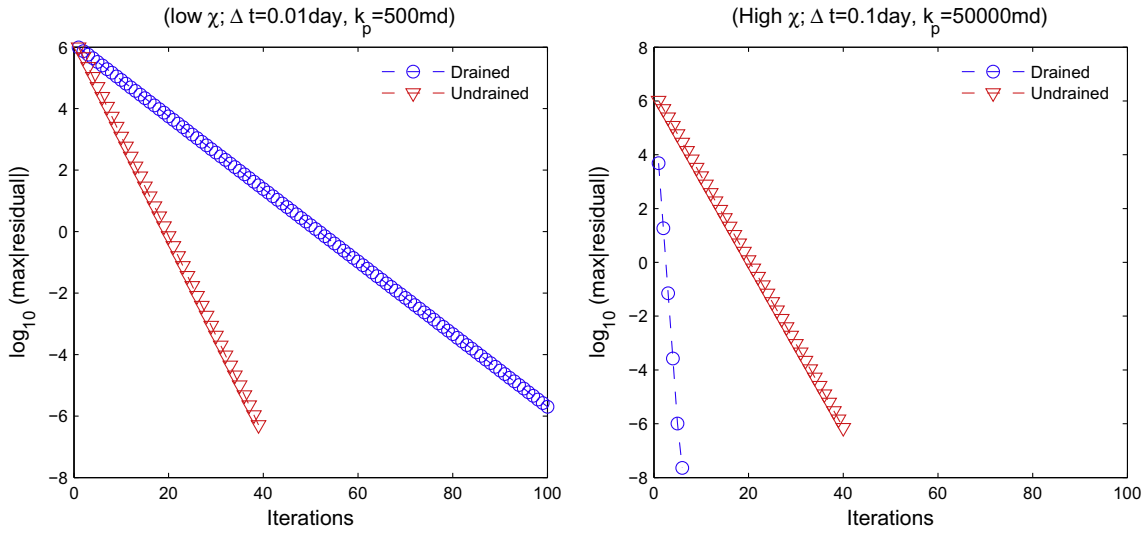

Fig. 20. Comparison of the rate of convergence at low (left) and high χ (right) for Case 2.1. The coupling strength τ is 0.95.

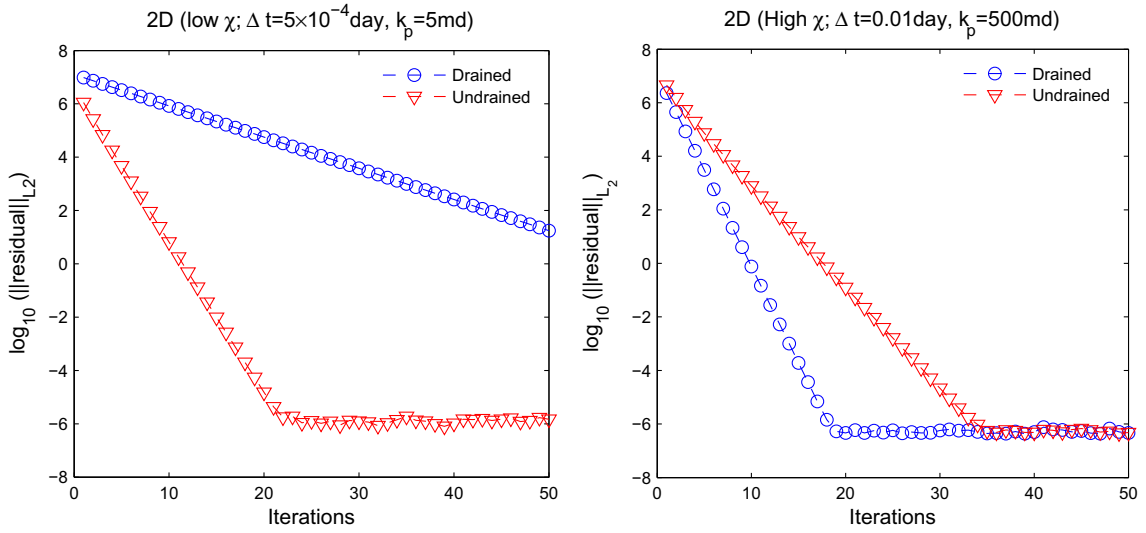

Fig. 21. Comparison of the rate of convergence at low (left) and high χ (right) for Case 2.2. The coupling strength τ is 0.77.

pling strength $\tau = 0.95$, where $c_f = 3.5 \times 10^{-8}\,\mathrm{Pa}^{-1}$. As shown in Fig. 20, the drained split yields a faster convergence rate for a large time step size $\Delta t = 0.1$ day and high permeability $k_p = 5 \times 10^4$ md (the right figure). In contrast, the undrained split shows better rate of convergence for a small time step size $\Delta t = 0.01$ day and low permeability $k_p = 500$ md (the left of Fig. 20). These results support the *a priori* estimates from Eqs. (107) and (121). Furthermore, the estimates and numerical results for the drained split also support the observation by Schrefler et al. [49] that a large time step size can reduce the spectral norm of the error amplification matrix for the drained split type of the staggered Newton scheme.

The 2-D results from Case 2.2 lead to the same conclusions as in Case 2.1. The coupling strength $\tau = 0.77$ with $c_f = 3.0 \times 10^{-9}\,\mathrm{Pa}^{-1}$. We perform two tests, corresponding to low and high diffusion of pressure. For low diffusion of pressure (i.e., low χ), the permeability and time step size are $k_p = 5$ md and $\Delta t = 5 \times 10^{-4}$ day, respectively. Fig. 21 (the left figure) shows that the rate of convergence for the undrained split is faster than the drained split in the case of low pressure diffusion. In contrast, the right of Fig. 21 shows that the rate of convergence for the drained split is faster than the undrained split because pressure is highly diffusive, where the permeability and time step size are $k_p = 500$ md and $\Delta t = 0.01$ day, respectively.

12. Conclusion

We have analyzed the stability of the drained and undrained splits, in combination with a generalized midpoint rule time discretization ($0 \leqslant \alpha \leqslant 1$), for the sequential solution of coupled flow and geomechanics. Following [26,30], we studied the stability properties by means of the von Neumann analysis for the linear case, and the energy method for the nonlinear case.

For the drained split, the backward Euler time discretization ($\alpha = 1$) is conditionally stable, and its stability is only a function of the coupling strength, independently of time step size. The method is unconditionally *unstable* when the midpoint rule time discretization ($\alpha = 0.5$) is used. A useful scheme in practice is a mixed time discretization, where $\alpha = 1$ for the mechanics step and $\alpha = 0.5$ for the flow step – the drained split with this time discretization has the same stability properties as the backward Euler scheme. The undrained split, in contrast, is unconditionally

stable – for any values of the coupling strength and time step size – as long as $\alpha \geqslant 0.5$.

We have also analyzed the nonlinear stability (or B-stability) of the undrained split via the energy method. The undrained split inherits the contractivity property of the continuum problem, which is a necessary (but not sufficient) requirement for algorithmic stability. We find that the generalized midpoint rule with $\alpha \geqslant 0.5$ is unconditionally *B*-stable, that is, contractive at discrete time level with respect to the natural norm of the coupled problem.

We also performed an analysis of the convergence properties of the drained and undrained splits with the backward Euler method using the matrix algebra method and spectral analysis. From the *a priori* estimates of error propagation, the drained split with a fixed number of iterations is not convergent in time even when it is stable. This lack of convergence is distinctive behavior of the coupled problem of flow and *quasi-static* mechanics; the drained split for fully-dynamic mechanics exhibits first-order accuracy with respect to time step size. The undrained split with a fixed number of iterations is convergent for a compressible system but becomes non-convergent when the system is quasi-incompressible ($M \to \infty$).

We also compared the drained and undrained splits in terms of the rate of convergence as a function of number of iterations, when full iterations are performed. Under a high pressure–diffusion condition (e.g., large time step size or high medium permeability), the drained split is faster than the undrained split, whereas the convergence of the undrained split is faster when the medium permeability is low or the time step size is small (low pressure–diffusion condition).

We have performed numerical experiments that support the *a priori* estimates of stability and convergence. In a separate paper [73], we investigate another type of sequential methods, in which the flow step is solved first. There, we show that a sequential method based on a fixed-stress split is unconditionally stable and overcomes the non-convergence and stiffness deficiencies of the undrained split for incompressible and quasi-incompressible systems.

Acknowledgments

The authors thank Prof. Ignacio Romero (Polytechnic University of Madrid) and Prof. Ronaldo Borja (Stanford University) for extended discussions on the analysis and implementation. Funding for this research was provided by the industrial affiliates of the Stanford University Petroleum Research Institute for Reservoir Simulation – SUPRI-B – and the Computer Modeling Group Foundation (to J. Kim and H.A. Tchelepi), and by Eni S.p.A., and the ARCO Chair in Energy Studies (to R. Juanes). This financial support is gratefully acknowledged.

References

[1] C. Truesdell, R.A. Toupin, The classical field theories, in: S. Flügge (Ed.), Principles of Classical Mechanics and Field Theory, Handbuch der Physik, vol. III/1, Springer-Verlag, Berlin, 1960, pp. 226–793.
[2] R. Waugh, E.A. Evans, Thermoelasticity of red blood-cell membrane, Biophys. J. 26 (1) (1979) 115–131.
[3] M. Kaczmarek, R.P. Subramaniam, S.R. Neff, The hydromechanics of hydrocephalus: steady-state solutions for cylindrical geometry, Bull. Math. Biol. 59 (2) (1997) 295–323.
[4] M.A. Biot, General theory of three-dimensional consolidation, J. Appl. Phys. 12 (1941) 155–164.
[5] O. Coussy, Mechanics of Porous Media, John Wiley and Sons, Chichester, England, 1995.
[6] H.F. Wang, Theory of Linear Poroelasticity, Princeton University Press, 2000.
[7] C.A. Barton, M.D. Zoback, D. Moos, Fluid flow along potentially active faults in crystalline rock, Geology 23 (8) (1995) 683–686.
[8] D. Wiprut, M.D. Zoback, Fault reactivation and fluid flow along a previously dormant normal fault in the northern North Sea, Geology 28 (7) (2000) 595–598.
[9] J.A. White, R.I. Borja, Stabilized low-order finite elements for coupled solid-deformation/fluid-diffusion and their application to fault zone transients, Comput. Methods Appl. Mech. Engrg. 197 (2008) 4353–4366.
[10] A.K. Jain, R. Juanes, Preferential mode of gas invasion in sediments: grain-scale mechanistic model of coupled multiphase fluid flow and sediment mechanics, J. Geophys. Res. 114 (2009) B08101, doi:10.1029/2008JB006002.
[11] R. Holtzman, R. Juanes, Crossover from fingering to fracturing in deformable disordered media, Phys. Rev. E 82 (2010) 046305, doi:10.1103/PhysRevE.82.046305.
[12] H.A. Merle, C.J.P. Kentie, G.H.C. van Opstal, G.M.G. Schneider, The Bachaquero study – a composite analysis of the behavior of a compaction drive/solution gas drive reservoir, J. Petrol Technol. (1976) 1107–1114.
[13] D. Kosloff, R.F. Scott, J. Scranton, Finite element simulation of Wilmington oil field subsidence: I. Linear modelling, Tectonophysics 65 (1980) 339–368.
[14] M.S. Bruno, Subsidence-induced well failure, SPE Drill. Eng. (1992) 148–152.
[15] J.T. Fredrich, J.G. Arguello, G.L. Deitrick, E.P. de Rouffignac, Geomechanical modeling of reservoir compaction, surface subsidence, and casing damage at the Belridge diatomite field, SPE Reserv. Eval. Eng. 3 (4) (2000) 348–359.
[16] A. Settari, F.M. Mourits, A coupled reservoir and geomechanical simulation system, Soc. Petrol Eng. J. 3 (3) (1998) 219–226.
[17] A. Settari, D.A. Walters, Advances in coupled geomechanical and reservoir modeling with applications to reservoir compaction, Soc. Petrol Eng. J. 6 (3) (2001) 334–342.
[18] M. Mainguy, P. Longuemare, Coupling fluid flow and rock mechanics: formulations of the partial coupling between reservoir and geomechanics simulators, Oil Gas Sci. Technol. 57 (2002) 355–367.
[19] S.E. Minkoff, C.M. Stone, S. Bryant, M. Peszynska, M.F. Wheeler, Coupled fluid flow and geomechanical deformation modeling, J. Petrol Sci. Eng. 38 (2003) 37–56.
[20] L.K. Thomas, L.Y. Chin, R.G. Pierson, J.E. Sylte, Coupled geomechanics and reservoir simulation, Soc. Petrol Eng. J. 8 (4) (2003) 350–358.
[21] D. Tran, A. Settari, L. Nghiem, New iterative coupling between a reservoir simulator and a geomechanics module, Soc. Petrol Eng. J. 9 (3) (2004) 362–369.
[22] R.H. Dean, X. Gai, C.M. Stone, S.E. Minkoff, A comparison of techniques for coupling porous flow and geomechanics, Soc. Petrol Eng. J. 11 (1) (2006) 132–140.
[23] B. Jha, R. Juanes, A locally conservative finite element framework for modeling coupled fluid flow and reservoir geomechanics, Acta Geotech. 2 (3) (2007) 139–153.
[24] R.W. Lewis, Y. Sukirman, Finite-element modeling of 3-phase flow in deforming saturated oil-reservoirs, Int. J. Numer. Anal. Methods Geomech. 17 (8) (1993) 577–598.
[25] R.W. Lewis, B.A. Schrefler, The Finite Element Method in the Static and Dynamic Deformation and Consolidation of Porous Media, second ed., John Wiley and Sons, Chichester, UK, 1998.
[26] F. Armero, Formulation and finite element implementation of a multiplicative model of coupled poro-plasticity at finite strains under fully saturated conditions, Comput. Methods Appl. Mech. Engrg. 171 (1999) 205–241.
[27] L. Jean, M. Mainguy, R. Masson, S. Vidal-Gilbert, Accelerating the convergence of coupled geomechanical-reservoir simulations, Int. J. Numer. Anal. Methods Geomech. 31 (2007) 1163–1181.
[28] K.C. Park, Stabilization of partitioned solution procedure for pore fluid–soil interaction analysis, Int. J. Numer. Meth. Engrg. 19 (11) (1983) 1669–1673.
[29] O.C. Zienkiewicz, D.K. Paul, A.H.C. Chan, Unconditionally stable staggered solution procedure for soil–pore fluid interaction problems, Int. J. Numer. Meth. Engrg. 26 (5) (1988) 1039–1055.
[30] F. Armero, J.C. Simo, A new unconditionally stable fractional step method for coupled thermomechanical problems, Int. J. Numer. Meth. Engrg. 35 (1992) 737–766.
[31] J.H. Prevost, Partitioned solution procedure for simultaneous integration of coupled-field problems, Commun. Numer. Methods Engrg. 13 (1997) 239–247.
[32] B.A. Schrefler, L. Simoni, E. Turska, Standard staggered and staggered Newton schemes in thermo-hydro-mechanical problems, Comput. Methods Appl. Mech. Engrg. 144 (1997) 93–109.
[33] M. Huang, O.C. Zienkiewicz, New unconditionally stable staggered solution procedures for coupled soil–pore fluid dynamic problems, Int. J. Numer. Meth. Engrg. 43 (1998) 1029–1052.
[34] C.A. Felippa, K.C. Park, Staggered transient analysis procedures for coupled mechanical systems: formulation, Comput. Methods Appl. Mech. Engrg. 24 (1980) 61–111.
[35] C. Farhat, K.C. Park, Y. Dubois-Pelerin, An unconditionally stable staggered algorithm for transient finite element analysis of coupled thermoelastic problems, Comput. Methods Appl. Mech. Engrg. 85 (1991) 349–365.
[36] F. Armero, J.C. Simo, A prior stability estimates and unconditionally stable product formula algorithms for nonlinear coupled thermoplasticity, Int. J. Plasticity 9 (1993) 749–782.
[37] J.C. Simo, Nonlinear stability of the time-discrete variational problem of evolution in nonlinear heat conduction, plasticity and viscoplasticity, Comput. Methods Appl. Mech. Engrg. 88 (1991) 111–131.
[38] A. Araújo, A note on B-stability of splitting methods, Comput. Visual. Sci. 6 (2004) 53–57.
[39] W.H. Hundsdorfer, M.L. Splijer, A note on B-stability of Runge–Kutta methods, Numer. Math. 36 (1981) 319–331.
[40] I. Romero, Thermodynamically consistent time-stepping algorithms for non-linear thermomechanical systems, Int. J. Numer. Meth. Engrg. 79 (2009) 706–732.

[41] R.D. Richtmyer, K.W. Morton, Difference Methods for Initial Value Problems, second ed., John Wiley and Sons, 1967.
[42] K.E. Brenan, S.L. Campbell, L.R. Petzold, Numerical Solution of Initial-Value Problems in Differential-Algebraic Equations, SIAM, Philadelphia, 1996.
[43] A. Chorin, T.R. Hughes, M.F. Mccraken, J.E. Marsden, Product formulas and numerical algorithms, Commun. Pure Appl. Math. (1978) 205–256.
[44] M.L. Lapidus, Generalization of the Trotter-Lie formula, Integr. Equat. Oper. Theor. 4/3 (1981) 366–413.
[45] E. Turska, K. Wisniewski, B.A. Schrefler, Error propagation of staggered solution procedures for transient problems, Comput. Methods Appl. Mech. Engrg. 114 (1994) 177–188.
[46] P.K. Vijalapura, S. Govindjee, An adaptive hybrid time-stepping scheme for highly non-linear strongly coupled Problems, Int. J. Numer. Meth. Engrg. 64 (2005) 819–848.
[47] P.K. Vijalapura, J. Strain, S. Govindjee, Fractional step methods for index-1 differential-algebraic equations, J. Comput. Phys. 203 (2005) 305–320.
[48] J.C. Simo, S. Govindjee, Nonlinear B-stability and symmetry preserving return mapping algorithms for plasticity and viscoplasticity, Int. J. Numer. Meth. Engrg. 31 (1991) 151–176.
[49] B.A. Schrefler, L. Simoni, E. Turska, Standard staggered and staggered Newton schemes in thermo-hydro-mechanical problems, Comput. Methods Appl. Mech. Engrg. 144 (1997) 93–109.
[50] P.A. Vermeer, A. Verruijt, An accuracy condition for consolidation by finite elements, Int. J. Numer. Anal. Methods Geomech. 5 (1981) 1–14.
[51] A. Ženišek, The existence and uniqueness theorem in Biot's consolidation theory, Aplik. Matem. 29 (1984) 194–210.
[52] J. Wan, L.J. Durlofsky, T.J.R. Hughes, K. Aziz, Stabilized finite element methods for coupled geomechanics–reservoir flow simulations, in: SPE Reservoir Simulation Symposium, Houston, TX (SPE 79694), 2003.
[53] P.J. Phillips, M.F. Wheeler, A coupling of mixed and continuous Galerkin finite element methods for poroelasticity I: the continuous-in-time case, Comput. Geosci. 11 (2007) 131–144.
[54] P.J. Phillips, M.F. Wheeler, A coupling of mixed and continuous Galerkin finite element methods for poroelasticity II: the discrete-in-time case, Comput. Geosci. 11 (2007) 145–158.
[55] J. Geertsma, The effect of fluid pressure decline on volumetric change of porous rocks, Trans. AIME 210 (1957) 331–340.
[56] R.I. Borja, On the mechanical energy and effective stress in saturated and unsaturated porous continua, Int. J. Solids Struct. 43 (6) (2006) 1764–1786.
[57] K. Aziz, A. Settari, Petroleum Reservoir Simulation, Elsevier, London, 1979.
[58] T.J.R. Hughes, The Finite Element Method: Linear Static and Dynamic Finite Element Analysis, Prentice-Hall, Englewood Cliffs, NJ, 1987.
[59] J. Kim, H.A. Tchelepi, R. Juanes, Stability, accuracy and efficiency of sequential methods for coupled flow and geomechanics, Soc. Petrol Eng. J. (2011), doi:10.2118/119084-PA.
[60] I. Aavatsmark, An introduction to multipoint flux approximations for quadrilateral grids, Comput. Geosci. 6 (2002) 405–432.
[61] E. Isaacson, H.B. Keller, Analysis of Numerical Methods, John Wiley and Sons, New York, 1966.
[62] J.C. Strikwerda, Finite Difference Schemes and Partial Differential Equations, SIAM, Philadelphia, PA, 2004.
[63] M.I. Miga, K.D. Paulsen, F.E. Kennedy, Von Neumann stability analysis of Biot's general two dimensional theory of consolidation, Int. J. Numer. Meth. Engrg. 43 (1998) 955–974.
[64] J.E. Marsden, T.J.R. Hughes, Mathematical Foundations of Elasticity, Prentice-Hall, Englewood Cliffs, NJ, 1983 (Reprinted with corrections, Dover, New York, 1994).
[65] J.C. Butcher, A stability property of implicit Runge–Kutta methods, BIT 15 (1975) 358–361.
[66] J.C. Simo, T.J.R. Hughes, Computational Inelasticity, Springer, New York, 1998.
[67] J.C. Simo, R.L. Taylor, Consistent tangent operators for rate dependent elastoplasticity, Comput. Methods Appl. Mech. Engrg. 38 (1985) 101–118.
[68] R.L. Taylor, J.C. Simo, A return mapping algorithm for plane stress elastoplasticity, Int. J. Numer. Meth. Engrg. 22 (1986) 649–676.
[69] V. Thomée, Galerkin Finite Element Methods for Parabolic Problems, Springer-Verlag, Berlin, 1997.
[70] E. Turska, B.A. Schrefler, On convergence condition of partitioned solution procedures for consolidation problems, Comput. Methods Appl. Mech. Engrg. 106 (1993) 51–63.
[71] G. Strang, Linear Algebra and its Applications, third ed., Brooks/Cole, 1988.
[72] R.I. Borja, S.R. Lee, Cam-clay plasticity, part I: implicit integration of elasto-plastic constitutive relations, Comput. Methods Appl. Mech. Engrg. 78 (1990) 49–72.
[73] J. Kim, H.A. Tchelepi, R. Juanes, Stability and convergence of sequential methods for coupled flow and geomechanics: fixed-stress and fixed-strain splits, Comput. Methods Appl. Mech. Engrg. 200 (13–16) (2011) 1591–1606.